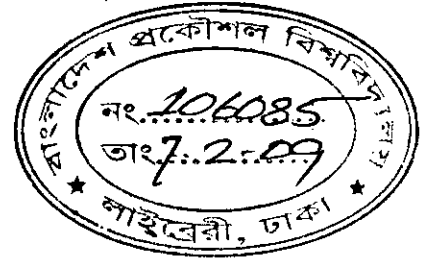


**OPERATING STRATEGIES OF A PHOTOVOLTAIC
GENERATOR EMBEDDED HIGH VOLTAGE POWER SYSTEM**

A thesis submitted to the Department of Electrical and Electronic Engineering in partial fulfillment of the requirements for the degree of
Master of Science in Electrical and Electronic Engineering (EEE)



By

MD. MOHSIN

Department of Electrical and Electronic Engineering (EEE)
BANGLADESH UNIVERSITY OF ENGINEERING AND TECHNOLOGY (BUET),
DHAKA.

December 2008



Declaration

This is to certify that this work has been done by the undersigned and it has not been submitted elsewhere for the award of any degree or diploma.

Signature of the Student

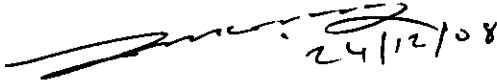


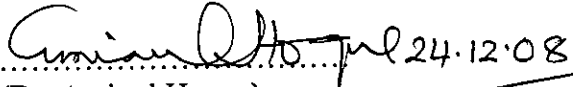
.....
(Md. Mohsin)




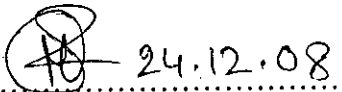
The thesis titled "Operating Strategies of a Photovoltaic Generator Embedded High Voltage Power System" submitted by Md. Mohsin, Roll: 040506139F, Session: April/2005, has been accepted as satisfactory in partial fulfillment of requirements for the degree of Master of Science in Engineering (Electrical and Electronic) on December 24, 2008.

BOARD OF EXAMINERS

1. 
.....
(Dr. S. Shahnawaz Ahmed)
Professor
Department of EEE, BUET, Dhaka
**Chairman
(Supervisor)**

2. 
.....
(Dr. Aminul Hoque)
Professor and Head
Department of EEE, BUET, Dhaka
Member (Ex-Officio)

3. 
.....
(Dr. Kazi Mujibur Rahman)
Professor
Department of EEE, BUET, Dhaka
Member

4. 
.....
(Dr. Mirza Golam Rabbani)
Professor
Department of EEE, RUET,
Rajshahi
Member (External)

Acknowledgments

This is a matter of great pleasure on the part of the author to acknowledge his deep sense of gratitude to his Supervisor Dr. S. Shahnawaz Ahmed, Professor of Department of Electrical and Electronic Engineering (EEE) and Dean of the Faculty of EEE, Bangladesh University of Engineering and Technology (BUET) for defining the research problem and his constant advice and guidance, encouragements and supports throughout the progress of this work.

The author thankfully acknowledges Professor Dr. Aminul Hoque the Head of the Dep. of EEE, BUET and Professor Dr. Shahidul Islam Khan the Director of Center for Energy Study (CES), BUET respectively for providing the computational facilities and the DIgSILENT software.

Abstract

This work has attempted to investigate into deriving operating strategies for a photovoltaic generator (PVG) embedded in a high voltage grid that can be applied for security analysis and generator dispatch in a power system with PVGs. Such investigations are yet to be reported in the literatures. The operating strategies have been recommended based on extensive simulation studies with appropriate load flow models of one or more PVGs (each $50 \text{ MW}_{\text{pk}}$ capacity) embedded at a voltage controlled bus or a specified real and reactive power bus in two test systems of different characteristics viz. a 138 kV 5-bus system (day peak 400 MW) and a 138 kV 14-bus system (day peak 780 MW).

Contents

Acknowledgments	iv
Abstract	v
List of Figures	viii
List of Tables	x
List of Principal Symbols and Abbreviations	xii
Chapter: 1 Introduction	1
1.1 General Considerations	1
1.2 Review of Literature	2
1.3 Objectives of the Present Research	3
1.4 Organization of the Thesis	4
Chapter: 2 Photovoltaic Generator and its Interfacing with the Grid System	5
2.1 Introduction	5
2.2 PVG Characteristic	6
2.3 Inverter Interface	9
2.3.1 Proposed method for predetermining inverter control parameters	13
2.4 Load Flow Analysis	17
2.5 Harmonic Power Flow Analysis	19
Chapter: 3 Results and Discussion	21
3.1 Introduction	21
3.2 Five Bus Test System and its Performance without Embedding Photovoltaic Generator (PVG)	22
3.3 Determining $V_{inv}-\phi_{inv}$ for the Control of the PVG Interfaced at a PV Bus in the 5-Bus System	24

3.3.1	Performance analysis for available currents from PVG	29
3.3.2	Variation of inverter power factor, bus specified voltage and angle, and modulation index with PVG current	34
3.3.3	Performance when same V_{inv} - ϕ_{inv} are specified in case of change in available PVG current	37
3.3.4	Performance with variation of system load	38
3.4	Performance Analysis under P_{inv} - Q_{inv} Control Mode of PVG Inverter Interfaced at a PV Bus in the 5-Bus System	42
3.5	Performance Analysis of PVG Interfaced at a PQ Bus in the 5-Bus System	45
3.6	Performance Analysis for 14-bus System with Embedded PVG	50
3.7	Analysis of Total Harmonic Distortion (THD) due to an embedded PVG	57
3.8	Summary of Operating Strategies for PVG Embedded Power System	62
Chapter: 4	Conclusion	65
4.1	Conclusion	65
4.2	Recommendations for Further Research	67
	References	68
	APPENDIX-A	69

List of Figures

Figure 2.1	Equivalent circuit of a photovoltaic cell	6
Figure 2.2	I-V characteristic of a single photovoltaic cell in the presence of light	9
Figure 2.3	A 6 pulse three phase inverter	10
Figure 2.4	Signals of a three phase PWM inverter (a) sinusoidal control signals and triangular carrier signal (b) phase and line to line output voltage	10
Figure 2.5	Magnitude and phase angle of the output voltage and control signal	12
Figure 2.6	A PVG embedded in a power system	13
Figure 2.7	Flowchart to determine V_{inv} and ϕ_{inv} of the PWM inverter for specified photovoltaic currents in the initial stage	16
Figure 3.1	Single line diagram of a five bus test system without embedding PVG (Bus 1: Slack, Bus 3: PV and remaining buses PQ type)	23
Figure 3.2	Variation of PV bus angle of the five bus test system with injected power	25
Figure 3.3	Photovoltaic generator interfaced at a PV bus of the 5-bus test system	27
Figure 3.4	Voltage magnitude of the AC side of the PWM inverter bus with respect to the difference between peak PVG current and available PVG current	28
Figure 3.5	Phase difference between the AC side of the PWM inverter bus and the PV bus of the test system with respect to the difference between peak PVG current and available PVG current	29
Figure 3.6	The active power and the reactive power generation of the slack bus generator versus PVG current	32
Figure 3.7	The active power and the reactive power losses in the system versus photovoltaic current	33
Figure 3.8	Variation of the power factor of the PWM inverter with PVG	34

current

Figure 3.9	The specified inverter AC side bus voltage and angle versus photovoltaic current	35
Figure 3.10	Modulation index of PWM inverter versus photovoltaic current	36
Figure 3.11	Specified inverter AC voltage versus modulation index	36
Figure 3.12	One line diagram of a 5-bus power system where PVG is interfaced at a PQ bus	46
Figure 3.13	Voltage profile for all buses with PVG at a PQ and at a PV bus in the 5-bus test system	49
Figure 3.14	MW loss in the system when PVG is interfaced at a PQ bus and at a PV bus	50
Figure 3.15	One line diagram of a 14 bus power system	51
Figure 3.16	Voltage profile at all buses in the 14-bus test system before and after interfacing the PVG for four cases with P_{inv} - Q_{inv} control mode of the inverter	56

List of Tables

Table 3.1	Load flow results of the power system without embedding PVG	23
Table 3.2	Variation of the PV bus angle with additional power injected at the PV bus in the 5-bus test system	24
Table 3.3	PWM inverter bus voltage (V_{inv}) and phase angle (ϕ_{inv}) and the PV bus phase angle (ϕ_{pv}) of the test system for selected photovoltaic currents	28
Table 3.4	Load flow results for various available currents from the PVG interfaced at a PV bus (bus no. 3) of the 5-bus test system and V_{inv} - ϕ_{inv} control mode of the PVG inverter	31
Table 3.5	Load flow solutions at a given load for change of PVG current without updating V_{inv} - ϕ_{inv} specifications for the inverter	38
Table 3.6	Load flow results at a given load for change of PVG current with the corresponding V_{inv} - ϕ_{inv} specifications for the inverter	38
Table 3.7	Load flow results for the variation in load (Δ_{Load}) from the day peak of 405 MW while PVG current is 5 kA and $V_{inv} = 1.0230$ p.u., $\phi_{inv} = -2.3955^\circ$	40
Table 3.8	Load flow results for the variation in load (Δ_{Load}) from the day peak of 405 MW while PVG current is 25 kA and $V_{inv} = 1.0320$ p.u., $\phi_{inv} = 3.1520^\circ$	41
Table 3.9	Results for P_{inv} - Q_{inv} control mode of the inverter for the PVG interfaced at a PV bus (bus no. 3)	43
Table 3.10	Load flow results for the variation in load (Δ_{Load}) from the day peak of 405 MW while PVG current is 24 kA and $P_{inv} = 48$ MW, $Q_{inv} = 2.4$ MVAR	44
Table 3.11	Load flow results for various available currents for the PVG interfaced at a PQ bus (bus no. 4) of the 5 bus test system and P_{inv} - Q_{inv} control mode of inverter	48
Table 3.12	Load flow results for variations in available current from the PVG interfaced at a PV bus (bus no. 6) of the 14 bus test system and V_{inv} - ϕ_{inv} control mode of inverter	53

Table 3.13	Load flow results for variations in available current from the PVG interfaced at a PV bus (bus no. 6) of the 14 bus test system and P_{inv} - Q_{inv} control mode of inverter	54
Table 3.14	MW loss in the 14 bus system before and after interfacing the PVG in four cases with P_{inv} - Q_{inv} control mode of the inverter	55
Table 3.15	Harmonic order and corresponding values of $\frac{(V_{LL})_h}{V_{DC}}$ for $m_a=0.8$ and $m_f=39$	59
Table 3.16	Percentage values of the harmonic voltage magnitudes in terms of fundamental frequency output voltage	60
Table 3.17	Voltage THD for all the buses while the PVG is interfaced at a PV bus (bus 3) of the 5-bus test system corresponding to harmonic generated as in Table 3.16	61
Table 3.18	Voltage THD for all the buses while the PVG is interfaced at a PQ bus (bus 4) of the 5-bus test system corresponding to harmonic generated as in Table 3.16	62
Table A.1	Line data of the 138 kV 5-bus system, base value = 100 MVA	69
Table A.2	P, Q and V at each bus of the 138 kV 5-bus system, base value = 100 MVA	69
Table A.3	Line data of the 138 kV 14-bus system, base value = 100 MVA	70
Table A.4	P, Q and V at each bus of the 138 kV 14-bus system, base value = 100 MVA	71

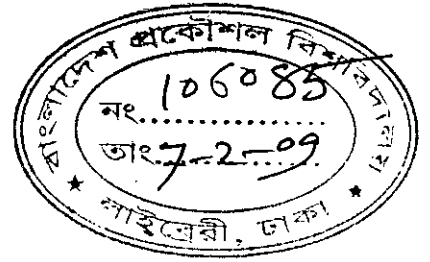
List of Principal Symbols and Abbreviations

PVG	Photovoltaic generator
PWM	Pulse Width Modulated
GTO	Gate Turn Off thyristor
THD	Total Harmonic Distortion
IEEE	Institution of Electrical and Electronics Engineers, Inc.
V_{inv}	Voltage magnitude of the inverter AC side bus
ϕ_{inv}	Phase angle of the inverter AC side
P_{inv}	Real power output of the inverter
Q_{inv}	Reactive power output of the inverter
I_{ph}	Short circuit current of a photovoltaic cell
I_{pho}	Short circuit current for a photovoltaic module / array
I_{pk}	Highest value of I_{pho} attainable at the maximum insolation i.e. the rated peak capacity of a photovoltaic array
V_{LL}	Line to line voltage
m_a	Amplitude modulation ratio of a PWM inverter
m_f	Frequency modulation ratio of a PWM inverter
$V_{control}$	Control or modulating signal of the PWM inverter

\hat{V}_{control}	Peak amplitude of the sinusoidal control signal v_{control} used in a PWM inverter
\hat{V}_{tri}	Peak amplitude of the triangular carrier signal of the PWM inverter
$(V_{\text{AN}})_1$	RMS value of the phase voltage of a PWM inverter at the fundamental frequency
$(V_{\text{LL}})_1$	Line to line rms voltage at the fundamental frequency
$(V_{\text{LL}})_h$	Line to line rms voltage at a harmonic frequency of order h
V_{DC}	Magnitude of the inverter DC bus voltage
P_{inject}	Injected active power at a PV bus from an external source or a PVG
φ_{PV}	Phase angle of the voltage controlled (PV) bus
δ	Phase angle difference between a PV bus and the AC bus of an inverter
$V_{\text{nom-pho}}$	Nominal voltage of a PVG
P_{spec}	Specified real power
J	Jacobian matrix
$\Delta\varphi$	Vector of the incremental phase angle
ΔV	Vector of the incremental voltage magnitude
φ_{PV_i}	Phase difference between a voltage controlled (PV) bus and another i th bus connected to this PV bus
P_{slack}	Real power generation of the slack bus generator
Q_{slack}	Reactive power generation of the slack bus generator

Chapter 1

Introduction



1.1 General Considerations

Apart from the apprehension of depleting fossil fuel reserve, the concern for global warming has become an impetus in the developed part of the world to integrate photovoltaic generators (PVG) with the conventional power grid system. In the developing part of the world the reason for using photovoltaic system is mainly the inability to supply electricity to the vast population from the conventional grid and thus there the photovoltaic is mainly used in the stand alone mode. In the long run there also the photovoltaic (where possible) is expected to be interfaced with the grid.

Desired DC power can be generated from a set comprising an appropriate number of series-parallel connected solar cells termed as the photovoltaic array [1]. Generated DC power is then converted to useful AC power by an inverter. The output AC power of the inverter is provided to the grid system through a step up transformer. Controlling the inverter is the main concern in interfacing the photovoltaic system with the grid. Due to less switching loss and less total harmonic distortion (THD) pulse width modulated (PWM) inverter [2] is preferable for interfacing a PVG with a grid system.

1.2 Review of Literature

In Germany, Australia and other developed countries large projects that involve addition of solar electricity ranging from 10 MW [3] to more than 150 MW [4] to the conventional high voltage grid are either already completed or expected to be commissioned in next few years. But no information is available on their operating strategies that could help utilities in planning, design and implementation of similar projects. The available literature on this subject is also inadequate.

In the work [5] a prototype was developed for a small photovoltaic module (only 110 W) interfaced with utility at 230 V through a 230 V \pm 10% tap changing transformer. The effects of changes of insolation from artificial sources and AC supply voltage on the behaviour of the photovoltaic module were observed through this experimental setup. However, the outcome of this small scale model will be difficult to be implemented and inadequate to be applied to predict in advance the performance of bulk solar power generating stations when interfaced with high voltage grids. So simulation studies are required for predicting the impacts of embedding a bulk photovoltaic generator on the operation of power systems.

In the work [6] unit commitment and economic dispatch were done out of academic interest to find the generation cost parameters in a 8-bus test system (peak demand 344 MW) in which a 6 MW peak photovoltaic and a 6 MW battery (only 1.8% of peak load) unit were considered to be interfaced. But as the battery storage is a very expensive option coupled with the photovoltaic module cost, the future practical power systems with large contributions from photovoltaic will exclude battery storage and reduce production cost by reserving a proportionate thermal generation capacity for use

at night. However, the work [6] does not address the control and operational performance of the photovoltaic embedded system.

1.3 Objectives of the Present Research

Load dispatching or steady state security assessment [7] of a conventional power system requires that a load flow analysis be made in advance considering various operating conditions and / or contingences (e.g. faults) in the system. The main difficulty for doing this in a PVG embedded power system is lack of appropriate model and method to predetermine the PVG control parameters and use those in load flow analysis. The present work focuses on the following.

- i) To predetermine the control parameters for operating a PVG interfaced with the grid system through a pulse width modulated (PWM) inverter.
- ii) To apply load flow analysis technique to determine the real and reactive power flows, the voltage profile, the system loss, total harmonic distortion (THD) at various buses and the modulation ratio of the inverter considering the embedded PVG's available capacity and varying the output of the conventional generators at a given day peak load.
- iii) To predict the performance of the PVG embedded grid system under dynamic conditions such as change in insolation and system loads.
- iv) To compare the effects of embedding a PVG at various types of buses in a conventional power system.

1.4 Organization of the Thesis

The presentation of the material studied in the present work is organized as follows.

Chapter 1 presents the review of the literature, objectives of the thesis along with the thesis organization.

Chapter 2 discusses the general characteristics of a photovoltaic generator, its modelling, the inverter control, load flow with AC and DC sources, and harmonic load flow. In this chapter an algorithm (real time compatible) has been proposed for the predetermination of the inverter control parameters.

Chapter 3 presents the results of extensive load flow simulation tests of two different systems viz. a 138 kV 5-bus system (day peak 400 MW) and a 138 kV 14-bus system (day peak 780 MW) considering variable load, insolation dependent PVG current capacity, type of interfacing grid buses (constant voltage or PQ) and different control modes for a PWM inverter. This also presents harmonic analysis for a PVG embedded in the 5-bus test system.

Chapter 4 presents the summary of the achievements made in the present work.

The appendixes provide supporting data and information.

Chapter 2

Photovoltaic Generator and its Interfacing with the Grid System

2.1 Introduction

Photovoltaic generator (PVG) is an insolation (incoming solar radiation) dependent DC electricity generator. Irregular solar irradiance makes a PVG an intermittent power generator. For a grid connected PVG a PWM inverter is used to convert the generated DC power into AC power at the grid frequency. However, this conversion also produces harmonics whose frequencies are multiples of the fundamental frequency i.e. the frequency of the grid with which the PVG is interfaced. The influence of the PVG on the grid system operation can be assessed and the operating strategies for such a system decided in advance and / or during operation through a load flow analysis. The load flow analysis for a conventional power system needs to be appropriately modified to model the inverter AC bus, inverter control parameters, the grid bus at which the inverter is interfaced and the PVG's variable capacity.

2.2 PVG Characteristics

A photovoltaic module consists of requisite number of cells connected in series parallel mode as to provide the desired current and voltage. So a photovoltaic cell is the basic building block of a photovoltaic module or an array of modules. A photovoltaic cell consists of a p-n junction semiconductor which shows I-V characteristic similar to that of a diode when biased in the dark (i.e. in absence of light). When light becomes incident on a photovoltaic cell without voltage bias (i.e. short circuited) it creates an electron-hole pair through absorbing photons with energy greater than the bandgap energy of the semiconductor [1-2]. These carriers create a short circuit current (I_{ph}) proportional to the incident radiation. When both light and voltage bias are present the single photovoltaic cell current I_c is the difference between the short circuit current and the dark current. Its equivalent circuit is shown in Figure 2.1. The circuit consists of a light-dependent DC current source and an internal shunt resistance R_{sh} and a series resistance R_s . The series resistance should be as low as possible and its shunt resistance should be very high, so that most of the available current can be delivered to the load. This is the reason that in many cases R_{sh} and R_s in the equivalent circuit are neglected.

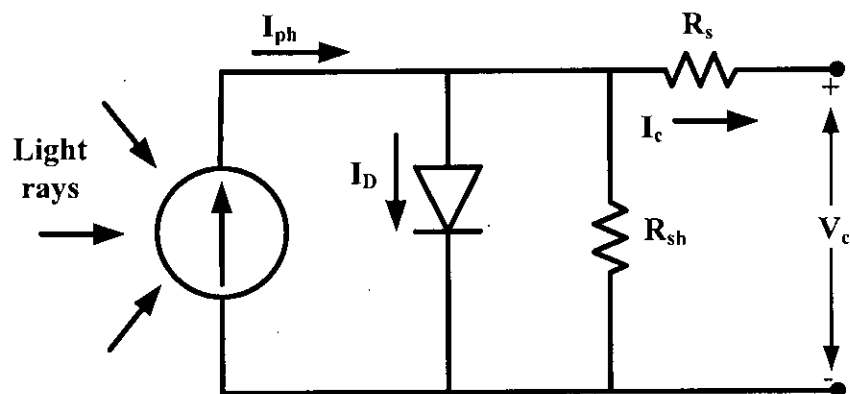


Figure 2.1 Equivalent circuit of a photovoltaic cell

A photovoltaic cell current I_c can be expressed by the following equations.

$$I_c = I_{ph} - I_D \quad (2.1)$$

where,

$$I_D = I_0 \left(e^{\frac{q(V_c + I_c R_s)}{nkT}} - 1 \right) \quad (2.2)$$

is the dark current

q ($=1.6 \cdot 10^{-19}$ coulomb) is the charge of an electron

V_c is the photovoltaic cell terminal voltage in loaded condition

k ($=1.38 \cdot 10^{-23}$ j / K) is the Boltzman constant

T is the cell temperature in °K

n ($=1$ or 2) is the diode quality factor

I_0 is the diode saturation current

I_{ph} is the insolation dependent photovoltaic cell current in short circuited condition

Equations (2.1) and (2.2) can be extended for a module or array taking into account the number of parallel connections of the photovoltaic cells. The notation for short circuit current for a module / array is I_{pho} as used in subsequent sections. The highest value of I_{pho} attainable at the maximum insolation is termed I_{pk} and that is also termed the rated peak capacity.

Figure 2.2 shows the I-V characteristic curves of a photovoltaic cell in the presence of light and voltage bias for three different temperatures [2]. It is shown that the cell current increases with solar irradiance (G , mW/cm^2). For a particular solar irradiance cell current remains constant up to certain limit after that cell current starts decreasing with increasing the cell voltage. The voltage upto which the cell current remains constant is termed in this work as the nominal voltage which is almost constant at various temperatures and insolation as in Figure 2.2. it is noteworthy that the knee point is the maximum power point. In general the voltage for the corresponding maximum power point is variable with temperature and insolation. The nominal voltage is less than the maximum voltage power point voltage as well as the open circuit voltage (zero photovoltaic current). It should be noted that the notions of nominal, maximum power point and open circuit voltage also hold good for an array consisting of many photovoltaic cells.

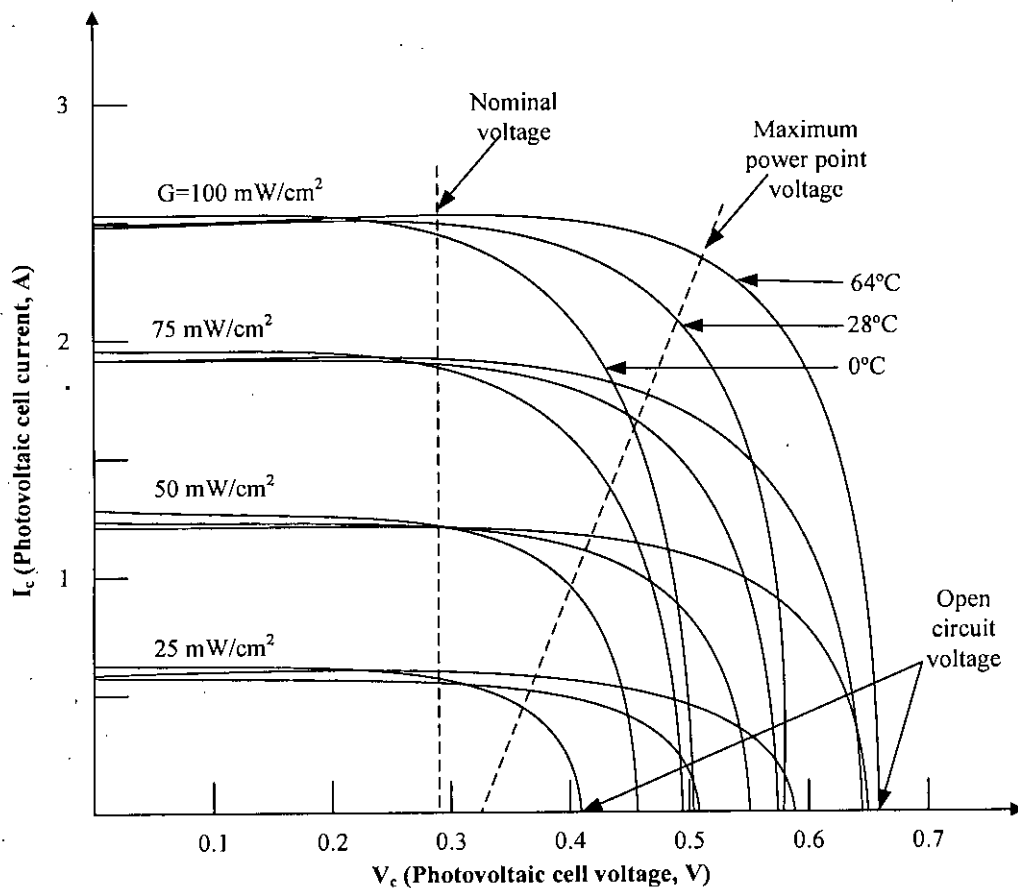


Figure 2.2 I-V characteristic of a single photovoltaic cell in the presence of light

2.3 Inverter Interface

A PVG is usually interfaced at a grid bus through a PWM inverter in which a switching signal is generated by comparing the desired sinusoidal output (i.e. the modulating signal or control signal) with high frequency triangular wave (carrier signal). The points of intersections of the modulating signal and the carrier signal are the points at which the GTOs or thyristors of the inverter are switched on by turn. Figure 2.3 shows a 6 pulse three phase inverter where V_{DC} is the input DC voltage (output voltage of the PVG) and V_{LL} is the output AC line voltage. Figure 2.4 shows the modulating, the carrier and the output AC voltage of a three phase PWM inverter.

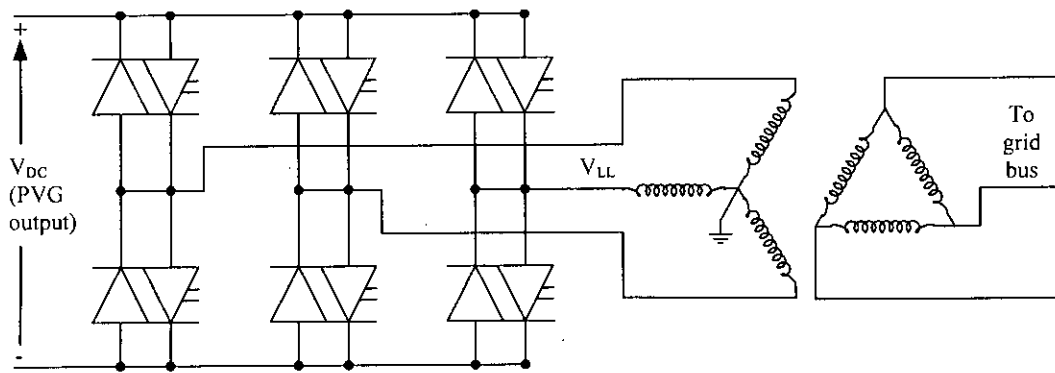


Figure 2.3 A 6 pulse three phase inverter

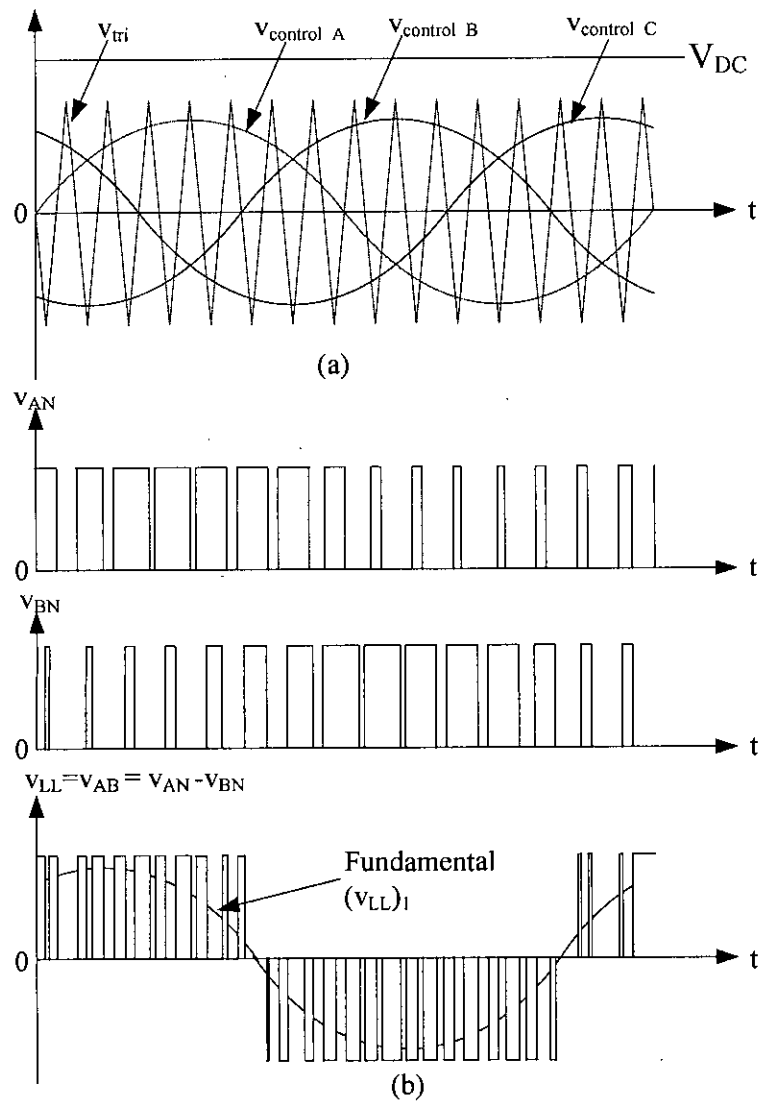


Figure 2.4 Signals of a three phase PWM inverter (a) sinusoidal control signals and triangular carrier signal (b) phase and line to line output voltage



The amplitude modulation ratio (m_a) of a PWM inverter is defined as [2]

$$m_a = \frac{\hat{V}_{\text{control}}}{\hat{V}_{\text{tri}}} \quad (2.3)$$

where,

\hat{V}_{control} is the peak amplitude of the sinusoidal control or modulating signal

v_{control}

\hat{V}_{tri} is the peak amplitude of the triangular carrier signal

$$v_{\text{control}} = \hat{V}_{\text{control}} \sin \omega_1 t \quad (2.4)$$

where,

$$\hat{V}_{\text{control}} \leq \hat{V}_{\text{tri}}$$

The fundamental frequency component of the PWM inverter output phase voltage $(v_{AN})_1$ is in phase with v_{control} for $m_a \leq 1.0$ [2] so that

$$(v_{AN})_1 = \frac{\hat{V}_{\text{control}}}{\hat{V}_{\text{tri}}} \sin \omega_1 t \frac{V_{DC}}{2} = m_a \sin \omega_1 t \frac{V_{DC}}{2} \quad (2.5)$$

Then $(\hat{V}_{AN})_1$ can be expressed as

$$(\hat{V}_{AN})_1 = m_a \left(\frac{V_{DC}}{2} \right) \quad (2.6)$$

which shows that in a sinusoidal PWM, the amplitude of the fundamental frequency component of the output voltage varies linearly with m_a (provided $m_a \leq 1.0$). Therefore, the range of m_a from 0 to 1 is referred to as linear range.

The line to line three phase rms voltage is then expressed as

$$\begin{aligned}
 (V_{LL})_1 &= \frac{\sqrt{3}}{\sqrt{2}} (\hat{V}_{AN})_1 \\
 &= \frac{\sqrt{3}}{\sqrt{2}} m_a \left(\frac{V_{DC}}{2} \right) \\
 &= 0.612 m_a V_{DC} \qquad (2.7)
 \end{aligned}$$

It should be noted that the fundamental component of the inverter output voltage $(v_{inv})_1$ can also be obtained with a phase shift ϕ_{inv} as in Figure 2.5 if the control signal has a phase shift of ϕ_{inv} . This can be done using a phase shifter for the control signal.

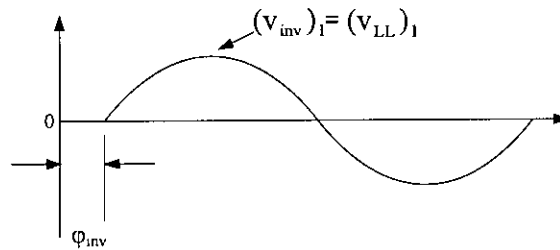


Figure 2.5 Magnitude and phase angle of the output voltage and control signal

2.3.1 Proposed Method for Predetermining Inverter Control Parameters

A PVG can be interfaced to a power system through a system bus which may be a voltage controlled PV (specified real power and voltage magnitude bus) or a PQ (specified real and reactive power injection i.e. difference between generation and load) bus. Figure 2.6 shows a PVG embedded power system. A blocking diode to protect the back flow to the PVG is implied. The PWM inverter's modulation index m_a needs to be adjusted for specified $V_{inv} \angle \phi_{inv}$ i.e. inverter AC bus voltage and phase angle or $P_{inv} - Q_{inv}$ i.e. specified real and reactive power output of the inverter. The former is termed $V_{inv} - \phi_{inv}$ control and the latter $P_{inv} - Q_{inv}$ control mode.

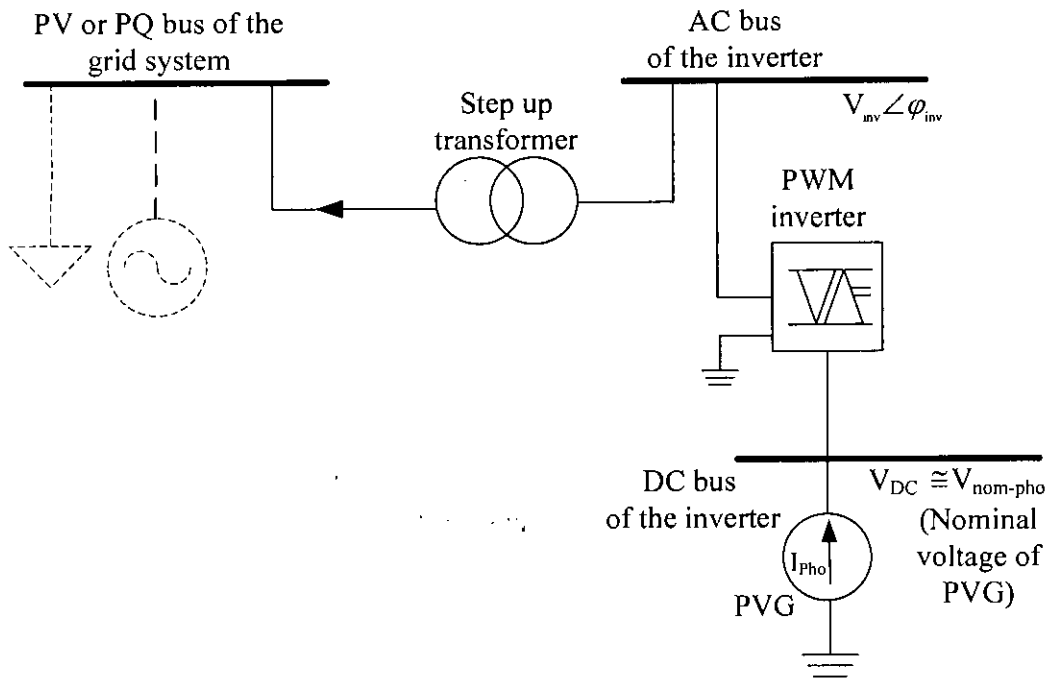


Figure 2.6 A PVG embedded in a power system

i) V_{inv}-φ_{inv} control mode:

A voltage controlled bus, also termed as PV bus, generally corresponds to a conventional generator where real or active power is fixed by turbine setting and voltage magnitude is fixed by automatic voltage regulator depending on the machine excitation. Power flow through a PV bus requires change in its voltage angle only. This change is linear in nature. PV bus angle decreases with decrease in injected power to PV bus. This relationship can be expressed as

$$\varphi_{PV} = a_1 P_{inject} + b_1 \quad (2.8)$$

The constants a_1 , b_1 of equation (2.8) can be determined considering various magnitudes of injected power from an external source at the PV bus and repeating the load flow analysis in each case. Then plotting the curve φ_{PV} vs P_{inject} the constants a_1 , b_1 can be determined.

Due to the voltage drop in the transformer, the voltage of the inverter AC bus should be specified higher than the voltage of the PV bus of the system with which the inverter is interfaced. The transfer of photovoltaic power (converted into AC) from inverter AC bus to the PV bus of the system depends on the inverter AC bus voltage magnitude and the difference of phase angles at the inverter AC and the PV buses. The relationship between V_{inv} and available photovoltaic current I_{pho} and that between φ_{inv} and φ_{PV} can also be expressed linearly as follows.

$$V_{inv} = a_2 \Delta I_{pho} + b_2 ; \quad I_{pho} > 0 \quad (2.9)$$

$$\partial = a_3 \Delta I_{pho} + b_3 \quad (2.10)$$

$$\varphi_{inv} = \varphi_{PV} + \partial \quad (2.11)$$

where,

ΔI_{pho} is the difference between peak photovoltaic current and available photovoltaic current i.e. $\Delta I_{pho} = I_{pk} - I_{pho}$

∂ is the phase difference between the AC bus of the inverter and the PV bus of the test system

The constants a_2 , b_2 , a_3 and b_3 of equations (2.9) to (2.11) can be determined using an algorithm proposed in the form of the flowchart in the Figure 2.7. Here V_{inv} and φ_{inv} are initially chosen slightly more than the V_{PV} and φ_{PV} i.e. the PV bus voltage magnitude and phase angle. The latter i.e. φ_{PV} is obtained using equation (2.8) for the intended power transfer equal to $P_{inject}^{(0)}$. The load flow is repeated unless the injectable power is approximately equal to the product of available an available photovoltaic current and the nominal PVG voltage. Thus the V_{inv} and φ_{inv} values are fixed for the chosen value of an available photovoltaic current I_{pho} . In this way another two sets of V_{inv} - φ_{inv} are obtained for two other values of I_{pho} .

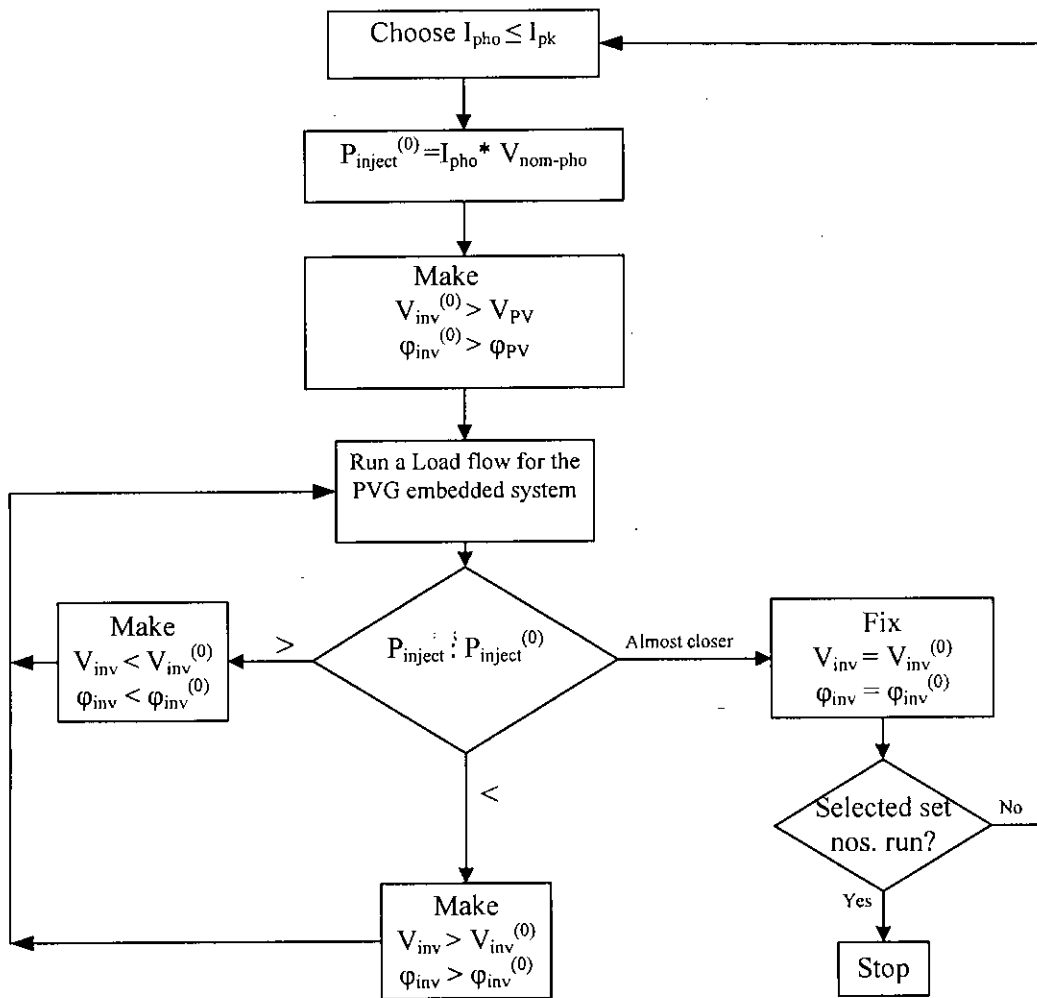


Figure 2.7 Flowchart to determine V_{inv} and ϕ_{inv} of the PWM inverter for specified photovoltaic currents in the initial stage

The V_{inv} vs ΔI_{ph0} and ∂ vs ΔI_{ph0} curves are plotted to determine the constants a_2 , b_2 , a_3 and b_3 . These constants are then substituted in equations (2.9) to (2.11). Finally using the set of four equations (2.8) to (2.11) V_{inv} - ϕ_{inv} can be computed readily for any new value of I_{ph0} without the need to execute the algorithm presented in the flow chart of Figure 2.7 for a given power system.

ii) P_{inv}-Q_{inv} control mode:

For P_{inv}-Q_{inv} control of the inverter P_{inv} can be specified by multiplying the available I_{pho} by V_{nom-pho} i.e. the nominal voltage of the PVG. Q_{inv} can be considered 5%-7% of P_{inv} to maintain a satisfactory power factor of the inverter.

It should be noted that due to uncontrolled voltage magnitude and angle of a PQ bus, V_{inv-φ_{inv}} control mode is not feasible for the inverter of a PVG interfaced at a PQ bus rather only P_{inv}-Q_{inv} control mode of PWM inverter is suitable. However, for a PVG interfaced at a PV bus either V_{inv-φ_{inv}} or P_{inv}-Q_{inv} control mode can be adopted for the inverter.

2.4 Load Flow Analysis

The equation used in each iteration k of basic Newton-Raphson's load flow [8] method is given by

$$\begin{bmatrix} \Delta\varphi \\ \Delta V \end{bmatrix}^{(k)} = \left[[J]^{-1} \right]^{(k)} \begin{bmatrix} \Delta P \\ \Delta Q \end{bmatrix}^{(k)} \quad (2.12)$$

where,

J is the full Jacobian matrix to be computed and inverted in each iteration

$\Delta\varphi$ is the vector of the incremental phase angles at all the PQ and PV buses

ΔV is the vector of the incremental voltage magnitudes of all the PQ buses

$$\Delta P = P_{\text{spec}} - P(V, \varphi) \quad \text{i.e. mismatch in active power at each PV and PQ}$$

bus

$$\Delta Q = Q_{\text{spec}} - Q(V, \varphi) \quad \text{i.e. mismatch in reactive power at each PQ bus}$$

In a PVG embedded power system the injected PVG power P_{inject} is fixed so long a particular insolation persists. Therefore P_{inject} can be considered in the specified power for a bus in the load flow analysis. In case of $V_{\text{inv}}-\varphi_{\text{inv}}$ control mode of the PVG inverter when interfaced at a PV bus the net specified real power of that PV bus can be represented as

$$P_{\text{spec, PV}} = (P_{\text{gen_PV}} - P_{\text{load_PV}} + P_{\text{inject}}) \quad (2.13)$$

where,

$$P_{\text{inject}} = I_{\text{pho}} V_{\text{nom-pho}}$$

Then the mismatch ΔP for the PV bus at where the PVG is connected is given by

$$\Delta P_{\text{PV}} = P_{\text{PV}} - V_{\text{PV}} \sum_{i=1}^{k+\text{inverter bus}} V_i (G_{\text{PV}_i} \cos \varphi_{\text{PV}_i} + B_{\text{PV}_i} \sin \varphi_{\text{PV}_i}) \quad (2.14)$$

where,

$$\varphi_{\text{PV}_i} = \varphi_{\text{PV}} - \varphi_i$$

when $i = \text{inverter bus}$ the phase angle $\varphi_i = \varphi_{\text{inv}}$ which is predetermined by equation (2.11) using the method mentioned in Sec. 2.3.1. Similarly $V_i = V_{\text{inv}}$ is also predetermined using equation (2.9) as in Sec. 2.3.1.

In case of the $P_{\text{inv}}\text{-}Q_{\text{inv}}$ control mode for the PVG inverter (interfaced at a PV or a PQ bus) its AC bus is included in the set of PQ buses of the grid system and then the load flow is done as usual.

2.5 Harmonic Power Flow Analysis

A PVG embedded power system is subjected to a load flow analysis for each of the considered harmonic frequency separately in a way similar to that at the fundamental frequency. However, in harmonic power flow analysis at the harmonic frequency (2nd and more) only the PVG inverter is the lone source while the conventional fundamental frequency producing generator are considered turned off. This means a large passive circuit is connected to the harmonic generator. The voltage magnitude of the harmonic source is to be specified for each harmonic order considered. The power flow analysis then gives voltage at other buses for each of the considered harmonic frequencies. Eventually the voltage THD at each bus is calculated using equation (2.15).

$$\text{THD} = \frac{1}{(V_{LL})_1} \sqrt{\sum_{h=2}^{\text{highest order}} (V_{LL})_h^2} \quad (2.15)$$

where,

$(V_{LL})_1$ = Line to line rms voltage at the fundamental frequency

$(V_{LL})_h$ = Line to line rms voltage at a harmonic frequency of order h

Chapter 3

Results and Discussion

3.1 Introduction

As mentioned in Chapter 2 a photovoltaic generator (PVG) which is by nature a nonlinear and variable DC current source can be interfaced at an AC power system through pulse width modulated (PWM) inverter. Since PVG represents a distributed generation resource, its effect has been analyzed by embedding it at a PV bus or a PQ bus of the test system and considering day peak load of the system. To derive the operating strategies for such a system analysis for various options are needed. So the load flow analysis of a PVG embedded power system has been done considering variable load, insolation dependent PVG current capacity, type of interfacing grid buses (PV or PQ) and different control modes for a PWM inverter (such as $V_{inv}-\phi_{inv}$ or $P_{inv}-Q_{inv}$ prespecified) in two test systems of different characteristics viz. 5-bus and 14-bus. Also Total Harmonic Distortion (THD) analysis was done for a representative case. A widely used power system software named DIGSILENT 13.0 has been used in the present work as a tool for this plethora of simulations. The software has no direct photovoltaic source model in its library but has DC current source ($I_{DC}=I_{pho}$), PWM inverter models etc. Analysis of a PVG embedded power system using DIGSILENT is not automatic rather requires user skill to model and integrate the power system and PVG components, predetermine the inverter control parameters and define the problem in an intelligent and appropriate way. However, use of an established and general

purpose software like DIgSILENT (instead of writing and using a prototype or customized source code) validates the simulations.

The findings of the extensive simulation tests have been presented in the form of quantitative results and general comments for typical cases in limited spaces.

3.2 Five Bus Test System and its Performance without Embedding Photovoltaic Generator (PVG)

In this work a five bus 138 kV power system [8] with an installed capacity of 600 MW and a day peak load of about 400 MW as shown in Figure 3.1 has been considered. Base values for the system is 100 MVA. Appendix-A.1 and A.2 give system data.

Table 3.1 shows the load flow results of the five bus system before embedding PVG. The load flow using full Newton-Raphson method converged in 3 iterations for a tolerance margin of 10^{-5} p.u.

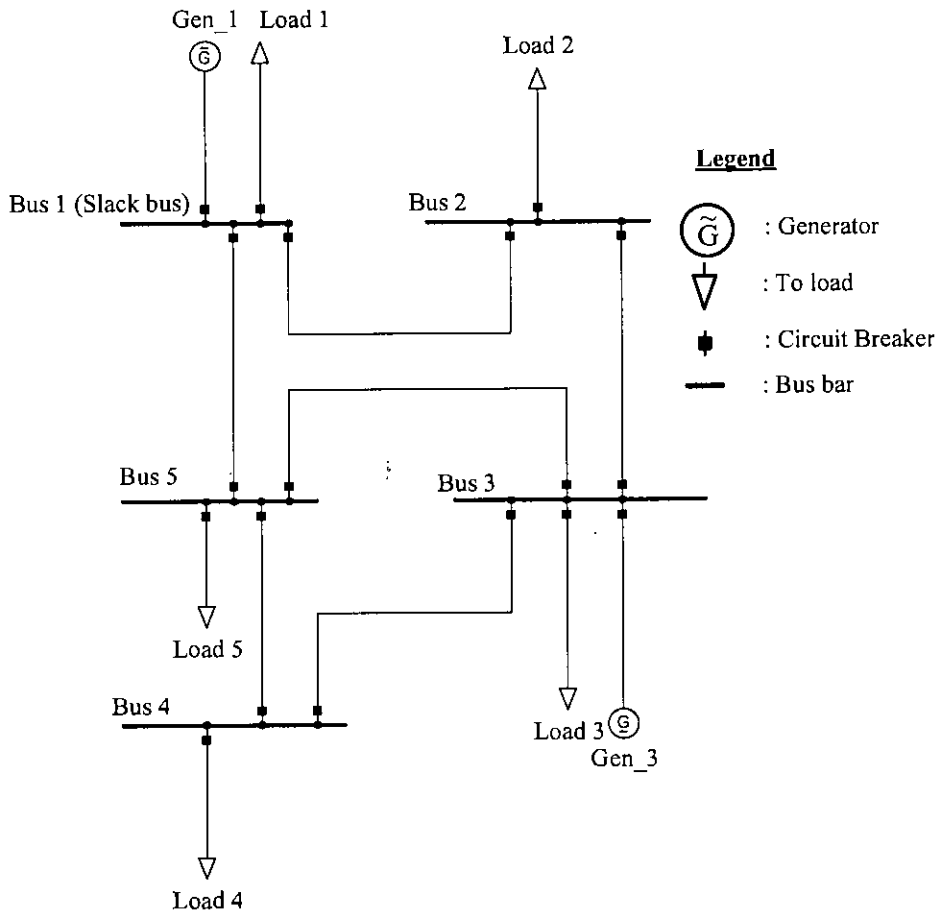


Figure 3.1 Single line diagram of a five bus test system without embedding PVG (Bus 1: Slack, Bus 3: PV and remaining buses PQ type)

Table 3.1 Load flow results of the power system without embedding PVG

Bus No.	Generation		Load		V (p.u.)	ϕ (deg)	Bus type	Total MW _{loss}	Total MVAR _{loss}
	P (MW)	Q (Mvar)	P (MW)	Q (Mvar)					
1	235.1073	105.9110	65	30	1.0400	0.0000	Slack	10.1405	26.0213
2	0	0	115	60	0.9597	-6.3259	PQ		
3	180	120.1047	70	40	1.0200	-3.7514	PV		
4	0	0	70	30	0.9100	-10.8787	PQ		
5	0	0	85	40	0.9630	-6.1421	PQ		

3.3 Determining $V_{inv}-\phi_{inv}$ for the Control of the PVG Interfaced at a PV Bus in the 5-Bus System

As mentioned in Sec. 2.3.1 the phase angle of a PV bus related as injected power P_{inject} using equation (2.8).

$$\phi_{PV} = a_1 P_{inject} + b_1 \quad (2.8)$$

To determine the constants a_1, b_1 of equation (2.8) various magnitudes of power were considered to be injected from an external source at the PV bus (bus 3) of the five bus test system and the load flow analysis done in each case. The corresponding phase angle of bus 3 is shown in Table 3.2.

Table 3.2 Variation of the PV bus angle with additional power injected at the PV bus in the 5-bus test system

Sl no.	Power injected at PV bus (bus 3) P_{inject} (MW)	PV bus angle ϕ_{PV} (deg)
1	40	-0.2246
2	20	-1.9792
3	10	-2.8630

Plotting the curve ϕ_{PV} vs P_{inject} as shown in Figure 3.2 the constants have been obtained as $a_1 = 0.0880, b_1 = -3.7514$:

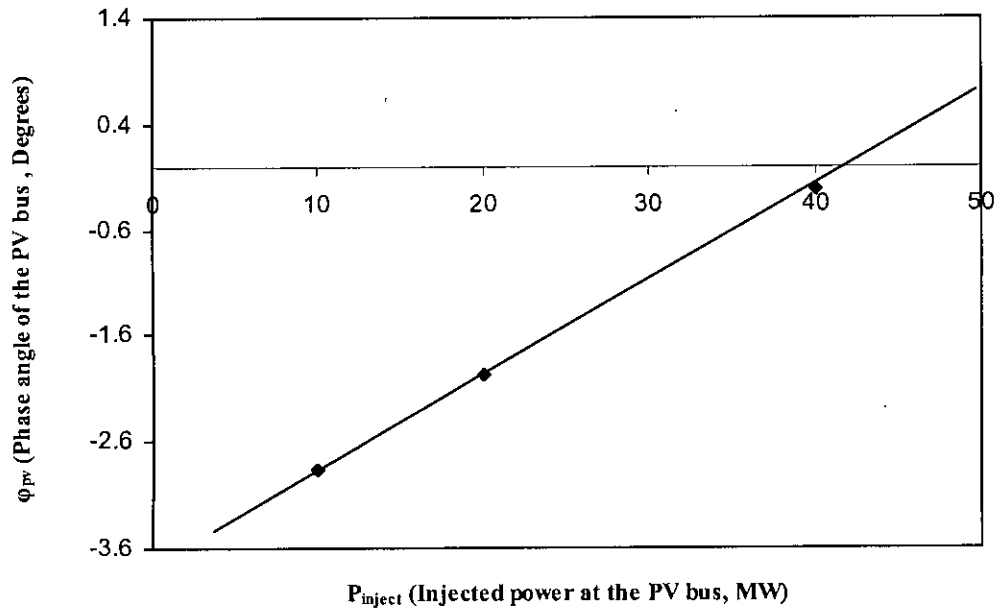


Figure 3.2 Variation of PV bus angle of the five bus test system with injected power

Figure 3.3 shows the one-line diagram of a PVG interfaced at a PV bus (bus no 3) of the test system. In this work a 50 MW, 25 kA peak capacity PVG with a nominal voltage of 2 kV has been considered to be interfaced through a 60 MVA PWM inverter and a 60 MVA of transformer. PVG is connected to the DC side of the inverter bus. The PWM inverter is connected between the DC side (PVG) bus and its AC side bus. Nominal AC voltage of the inverter bus (V_{inv}) is 1 kV. A 60 MVA, 6% (impedance) and 1/138 kV transformer is connected between the AC side of the inverter bus and the PV bus of the test system.

As mentioned in Chapter 2 the voltage drop in the transformer is to be considered and the amount of this drop depends on the amount of power transfer i.e. the current flow through it. So it is required to keep the AC side of the inverter bus voltage level higher than the PV bus of the system. The transfer of photovoltaic power from the

AC side of the inverter bus to the PV bus of the test system depends on the inverter AC bus voltage magnitude and the difference of phase angles at the inverter and the PV buses.

In the $V_{inv}-\phi_{inv}$ control mode of the PWM inverter AC bus voltage magnitude and phase angle are specified. On the basis of the theory developed in the Chapter 2 the magnitude and the phase angle of the AC side of the inverter bus voltage and angle for a particular insolation are calculated using equations (2.8), (2.9), (2.10) and (2.11) rewritten below.

$$\varphi_{PV} = a_1 P_{inject} + b_1 \quad (2.8)$$

$$V_{inv} = a_2 \Delta I_{pho} + b_2; \quad I_{pho} > 0 \quad (2.9)$$

$$\partial = a_3 \Delta I_{pho} + b_3 \quad (2.10)$$

$$\varphi_{inv} = \varphi_{PV} + \partial \quad (2.11)$$

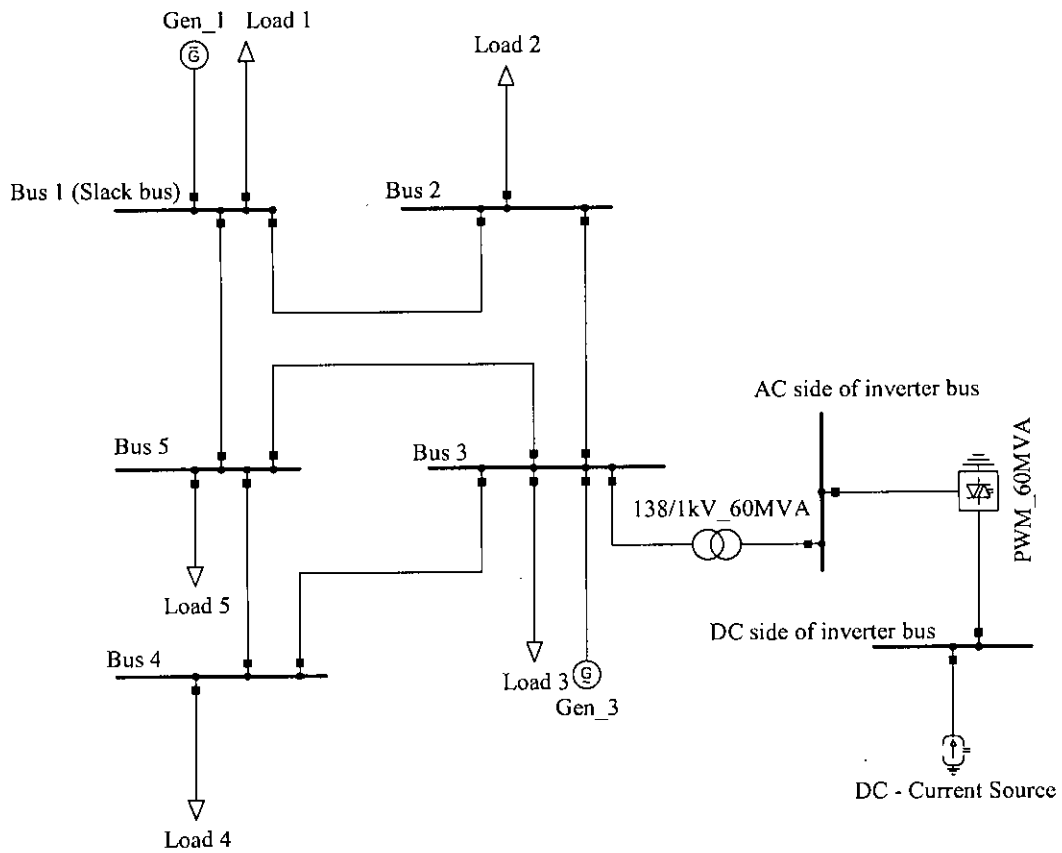


Figure 3.3 Photovoltaic generator interfaced at a PV bus of the 5-bus test system

As mentioned in Sec. 2.3.1, the obtained V_{inv} , ϕ_{inv} and P_{inject} for three selected values of I_{pho} are shown in Table 3.3. Substituting the values of P_{inject} in equation (2.8) ϕ_{PV} is obtained corresponding to each P_{inject} .

Table 3.3 PWM inverter bus voltage (V_{inv}) and phase angle (ϕ_{inv}) and the PV bus phase angle (ϕ_{PV}) of the test system for selected photovoltaic currents

Sl no.	I_{pho} (kA)	$\Delta I_{pho} = (I_{pk} - I_{pho})$ (kA)	Specified V_{inv} (p.u.)	Specified ϕ_{inv} (deg)	Amount of power transfer from PWM inverter to the PV bus of the test system P_{inject} (MW)	Phase angle of the PV bus of the test system ϕ_{PV} (deg)	Phase difference between the AC side of the inverter bus and the PV bus of the test system δ (deg)
1	25	0	1.0320	3.1520	48.9147	0.5531	2.5989
2	20	5	1.0297	1.7850	39.2488	-0.2975	2.0825
3	15	10	1.0275	0.4040	29.4863	-1.1566	1.5606

Plotting the curves V_{inv} vs ΔI_{pho} (Difference between peak photovoltaic current and available photovoltaic current) as in Figure 3.4 and δ vs ΔI_{pho} as in Figure 3.5 the constants have been obtained as $a_2 = -4.5 \times 10^{-4}$, $b_2 = 1.0320$ and $a_3 = -0.1039$, $b_3 = 2.5989$.

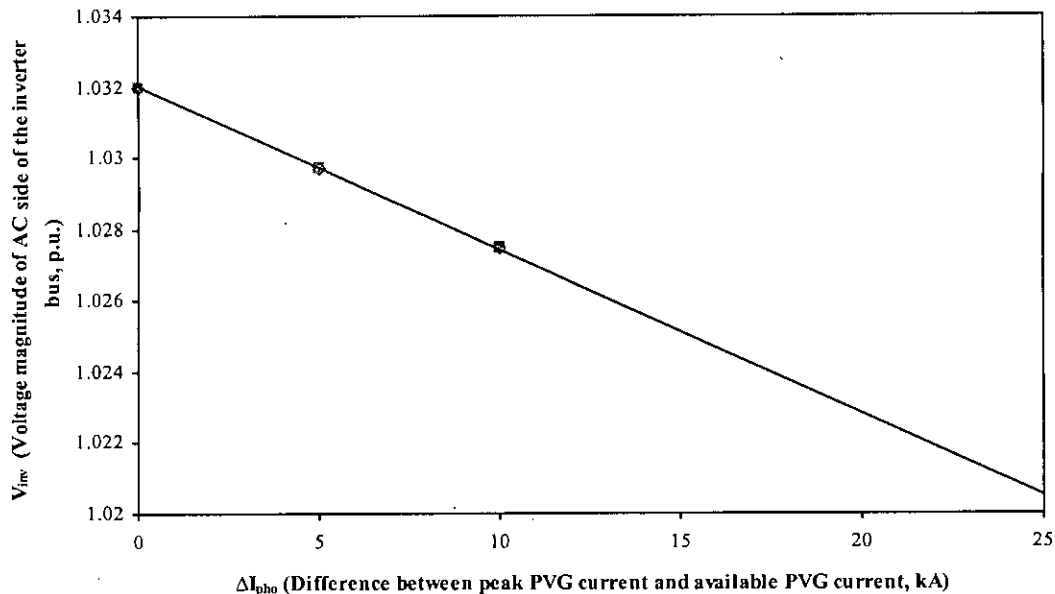


Figure 3.4 Voltage magnitude of the AC side of the PWM inverter bus with respect to the difference between peak PVG current and available PVG current

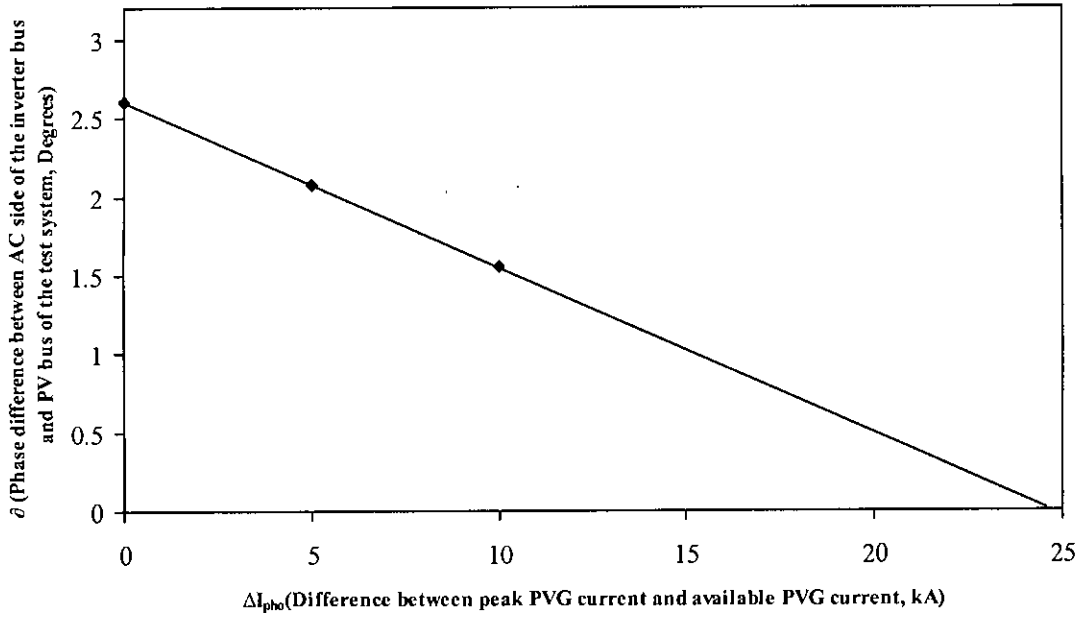


Figure 3.5 Phase difference between the AC side of the PWM inverter bus and the PV bus of the test system with respect to the difference between peak PVG current and available PVG current

3.3.1 Performance Analysis for Available Currents from PVG

On substituting values of the constants $a_1, b_1, a_2, b_2, a_3, b_3$, obtained in section 3.3 equations (2.8) to (2.11) become respectively as in equations (3.1) to (3.4)

$$\varphi_{PV} = 0.0880 * P_{inject} + (-3.7514) \quad (3.1)$$

$$V_{inv} = (-4.5 \times 10^{-4}) * \Delta I_{pho} + 1.0320; \quad I_{pho} > 0 \quad (3.2)$$

$$\partial = (-0.1039) * \Delta I_{pho} + 2.5989 \quad (3.3)$$

$$\varphi_{inv} = \varphi_{PV} + \partial \quad (3.4)$$

Table 3.4 shows the load flow results corresponding to different pairs of V_{inv} - ϕ_{inv} specifications. Each pair has been computed using equations (3.1) to (3.4) corresponding to available PVG short circuit current (I_{pho}). The load flow converged in 6 iterations. The Table lists amount of active (P_{inv}) and reactive (Q_{inv}) power output of PWM inverter, amplitude modulation index (m_a) of the PWM inverter, power factor (PF_{inv}) of the PWM inverter, net system loss in MW (MW_{loss}) and MVAR ($MVAR_{loss}$), bus-voltage magnitude in per unit and phase angle for each bus except the slack bus, active (P_{slack}) and reactive (Q_{slack}) power generation of slack bus generator.

Table 3.4 Load flow results for various available currents from the PVG interfaced at a PV bus (bus no. 3) of the 5-bus test system and V_{inv} - ϕ_{inv} control mode of the PVG inverter

Sl no.	I_{pho} (kA)	Specified V_{inv} (p.u.)	Specified ϕ_{inv} (deg)	m_a	PF_{inv}	P_{inv} (MW)	Q_{inv} (MVAR)	P_{slack} (MW)	Q_{slack} (MVAR)	$P_{Gen 3}$ (MW)	$Q_{Gen 3}$ (MVAR)	Total MW_{loss}	Total $MVAR_{loss}$
1	2	3	4	5	6	7	8	9	10	11	12	13	14
1	24	1.0315	2.8820	0.8609	0.9943	47.3446	5.0410	187.3699	112.2214	180	107.8678	10.3681	20.0892
2	16	1.0279	0.6830	0.8507	0.9941	31.4876	3.3628	203.0722	109.7269	180	111.0477	10.0733	20.7746
3	10	1.0252	-0.9880	0.8441	0.9933	19.5558	2.2744	215.0755	108.0985	180	113.8631	10.0755	21.9615
4	5	1.0230	-2.3955	0.8393	0.9879	9.5895	1.5328	225.2279	106.9074	180	116.4484	10.2282	23.3558
5	1	1.0213	-3.5299	0.8361	0.8326	1.6150	1.0745	233.4358	106.0684	180	118.6491	10.4359	24.7174

Table 3.4 (extended)

Sl no.	I_{pho} (kA)	V_2 (p.u.)	ϕ_2 (deg)	V_3 (p.u.)	ϕ_3 (deg)	V_4 (p.u.)	ϕ_4 (deg)	V_5 (p.u.)	ϕ_5 (deg)
		15	16	17	18	19	20	21	22
1	24	0.9604	-3.9773	1.02	0.3848	0.9122	-8.0351	0.9699	-4.3211
2	16	0.9603	-4.7528	1.02	-0.9833	0.9124	-8.9732	0.9647	-4.9222
3	10	0.9602	-5.3435	1.02	-2.0238	0.9124	-9.6883	0.9645	-5.3880
4	5	0.9600	-5.8419	1.02	-2.9007	0.9124	-10.2920	0.9642	-5.7666
5	1	0.9598	-6.2441	1.02	-3.6076	0.9123	-10.7795	0.9636	-6.0786

Figure 3.6 shows variation of slack bus active and reactive power generation with PVG current. Since the PVG injects real power into the system slack generator has to generate less real power. The total active power loss shows a decreasing trend with increase in the PVG current up to a certain level as shown in Figure 3.7. Then it slightly increases because the inverter switching loss usually varies nonlinearly with the input DC i.e. the PVG current. Since the generator of the PV bus (Bus 3) generates less reactive power with increase in PVG current and hence the reactive power transferred from the PVG, generator of the slack bus generates more reactive power. However, the total reactive power loss in the system decreases with increase in PVG current as shown in Figure 3.7.

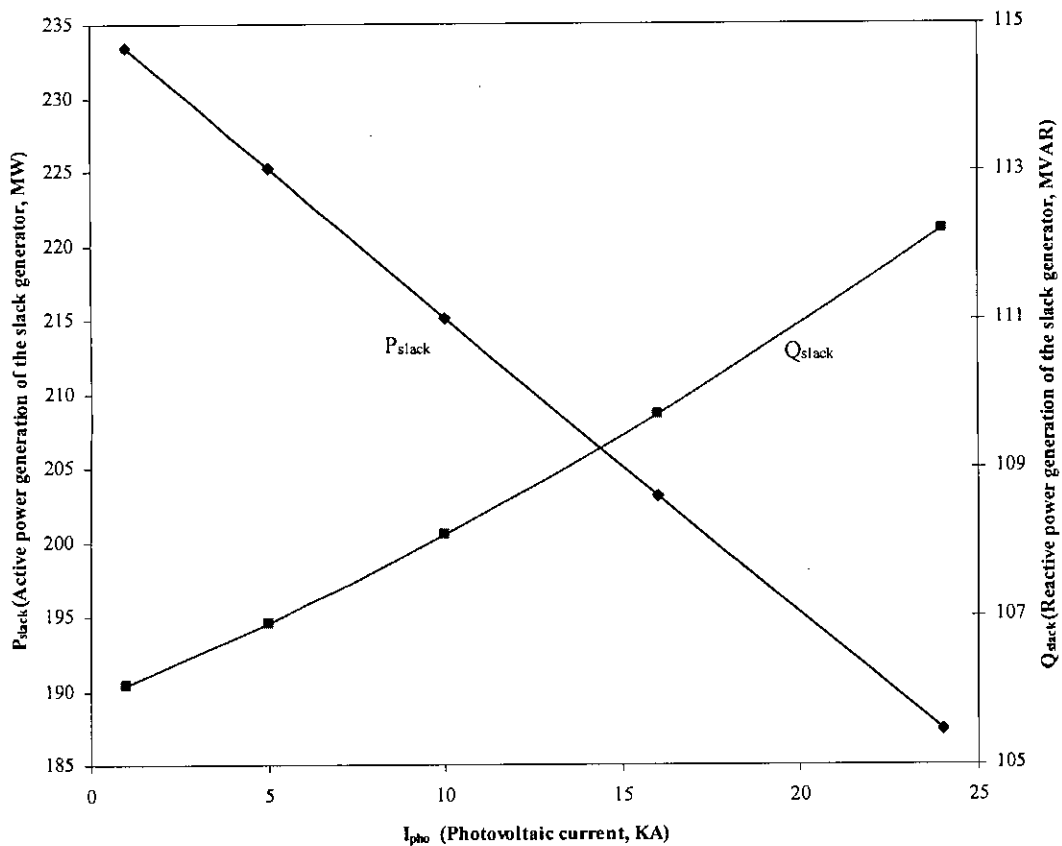


Figure 3.6 The active power and the reactive power generation of the slack bus generator versus PVG current

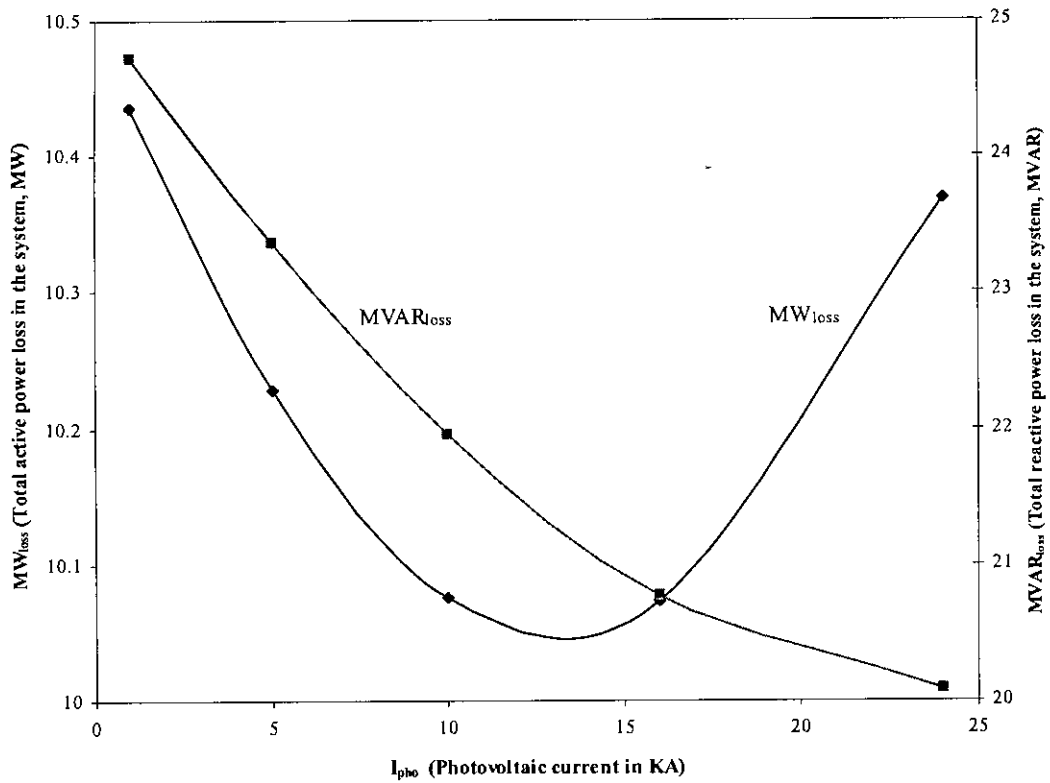


Figure 3.7 The active power and the reactive power losses in the system versus photovoltaic current

The voltage magnitudes of all the PQ buses and AC side of the inverter bus excepting bus 4 increase slightly with PVG current while all the bus voltage phase angles increase with increase in PVG current. The PQ bus 4 being further away from the PVG interfaced bus i.e. bus 3, experiences slightly nonlinear variation in voltage magnitude with increase in the PVG current.

3.3.2 Variation of Inverter Power Factor, Bus Specified Voltage and Angle, and Modulation Index with PVG Current

The power factor of the inverter is $\cos(\tan^{-1} \frac{Q_{inv}}{P_{inv}})$. Figure 3.8 shows an abrupt variation of the power factor in the lower range of PVG current while a gradual change (almost small variation) with the higher range of PVG current.

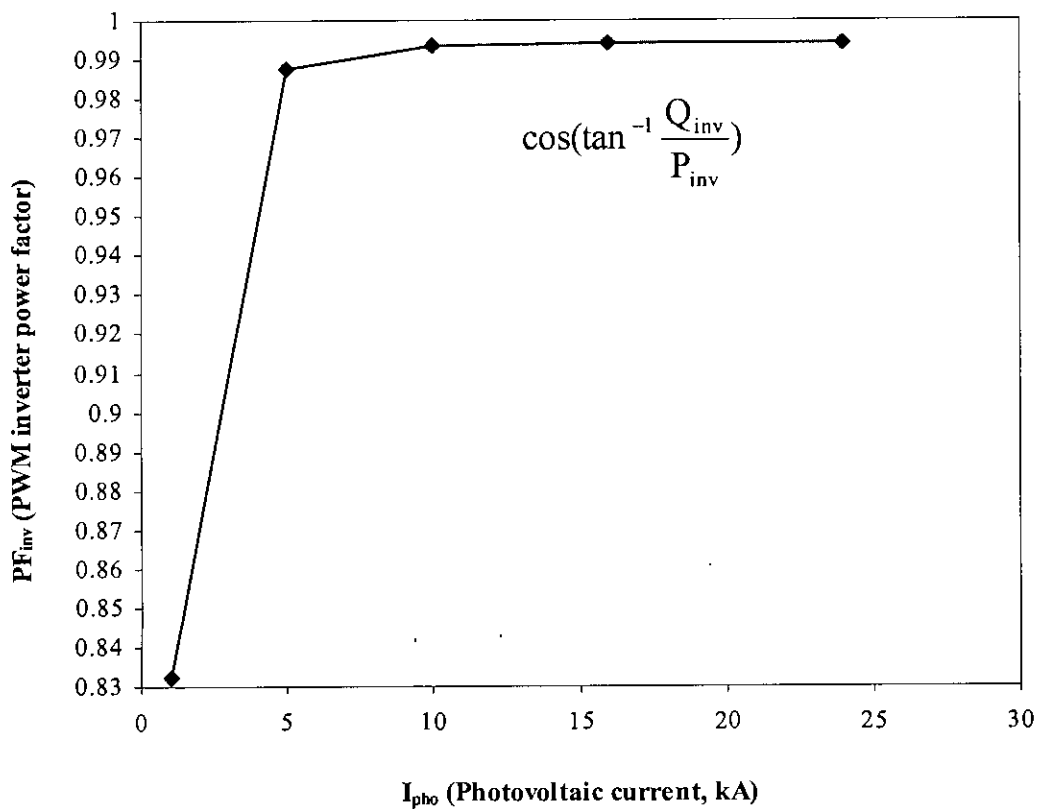


Figure 3.8 Variation of the power factor of the PWM inverter with PVG current

Figure 3.9 shows that the specified inverter AC side voltage V_{inv} and angle ϕ_{inv} increase linearly with the PVG current.

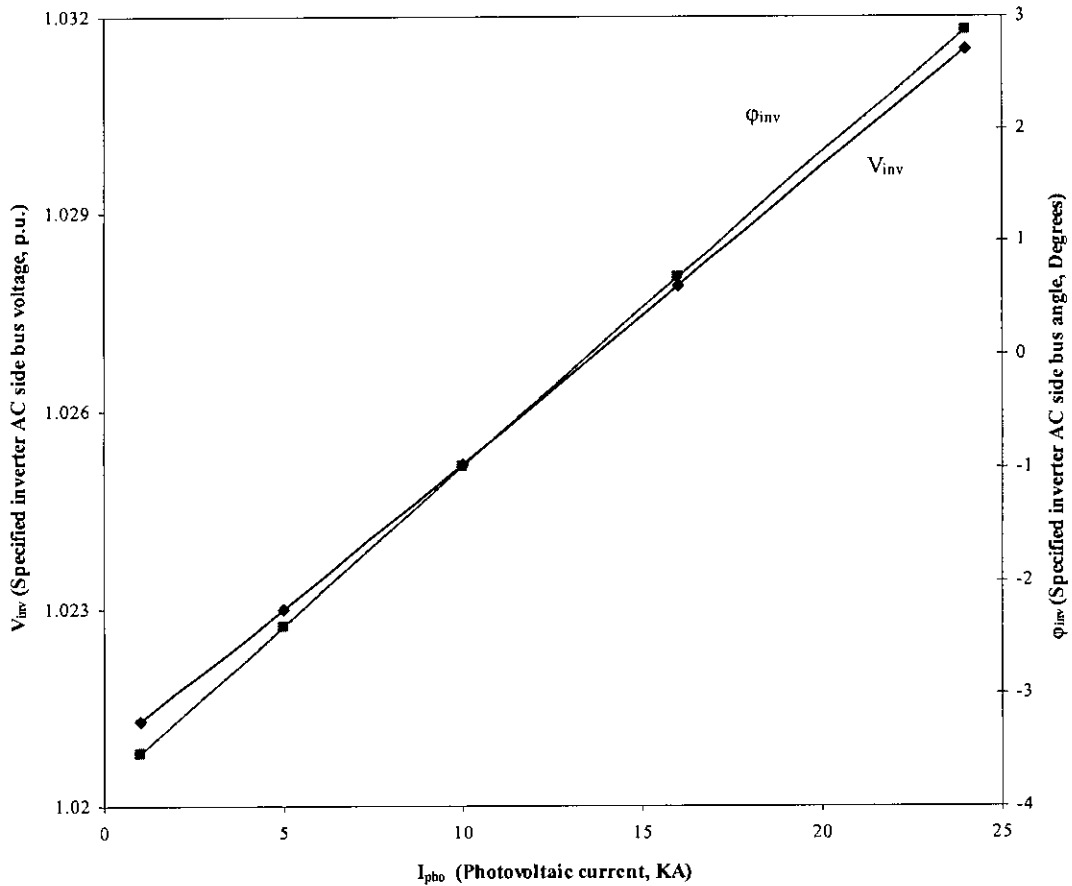


Figure 3.9 The specified inverter AC side bus voltage and angle versus photovoltaic current

Unlike specified V_{inv} and ϕ_{inv} , the modulation index of the PWM inverter increases slightly with PVG current as in Figure 3.10. It can also be observed that for the specified V_{inv} - ϕ_{inv} sets this index does not exceed unity and hence complies with the operational constraint of a sine PWM inverter. Also the inverter voltage V_{inv} will be in phase with the control signal or modulating sine wave. Figure 3.11 shows that the specified inverter AC voltage varies almost proportionately with the modulation index m_a so long $m_a < 1.0$.

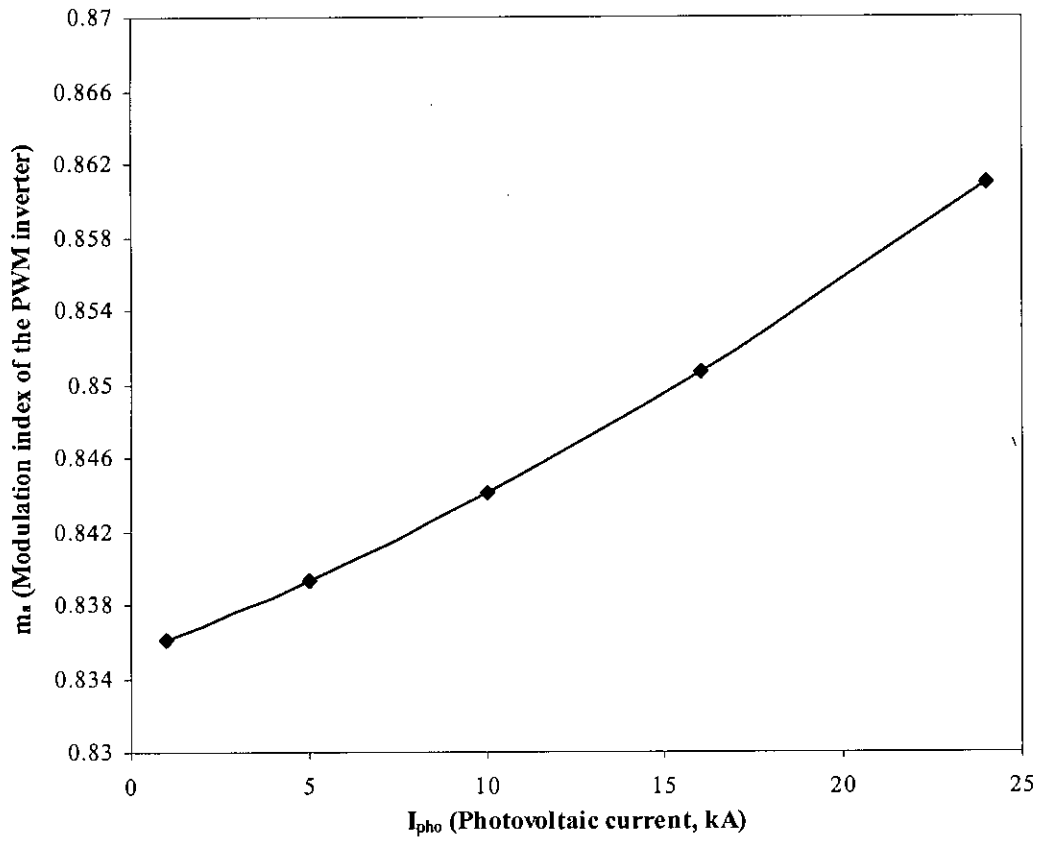


Figure 3.10 Modulation index of PWM inverter versus photovoltaic current

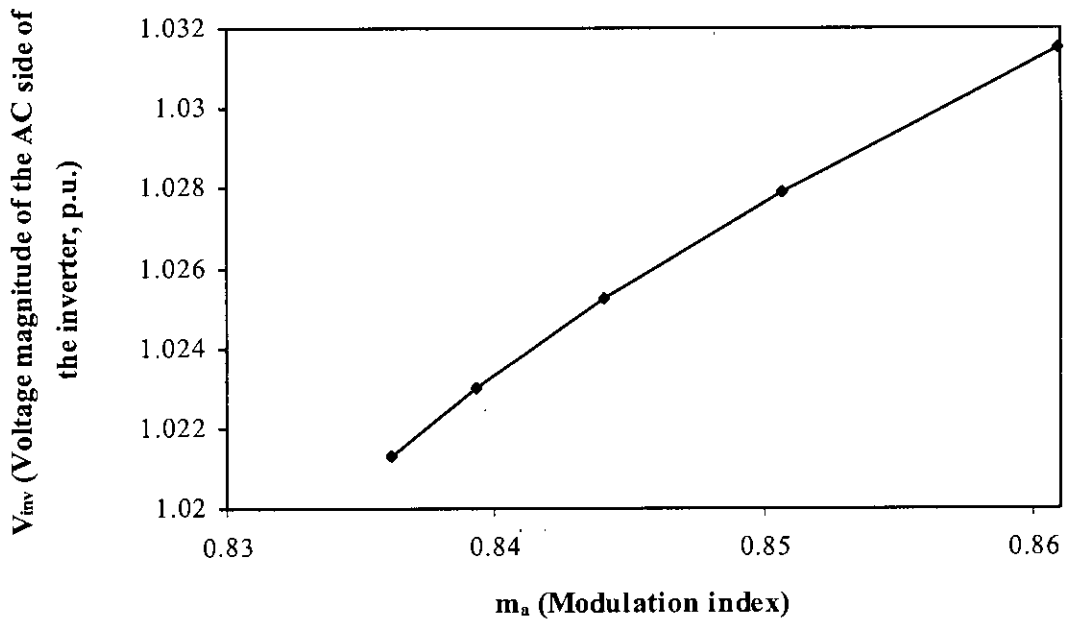


Figure 3.11 Specified inverter AC voltage versus modulation index

3.3.3 Performance when Same $V_{inv}-\phi_{inv}$ are Specified in Case of Change in Available PVG Current

To investigate into the effects of using the same $V_{inv}-\phi_{inv}$ for the inverter when the available PVG current changes depending upon insolation, several simulations were done. A representative case is shown in Table 3.5 and 3.6 for $\pm 20\%$ variation in the base $I_{ph0} = 5$ kA.

Table 3.5 shows the results for a $V_{inv} = 1.0230$ p.u. and a $\phi_{inv} = -2.3955^\circ$ (obtained using equations 3.1 to 3.4) specifications for the inverter control where the PVG current was 5 kA. If those specifications were not updated as seen in Table 3.5, the modulation index becomes low or exceeds unity value in some cases when the PVG current varies between 4 kA to 6 kA ($\pm 20\%$). However, it causes same real and reactive power transfer to the system but with a slightly disproportionate variation in the real power loss. On the other hand, updating $V_{inv}-\phi_{inv}$ with a change in the PVG current improves significantly the real and reactive power loss as well as power transfer to the system, the inverter power factor and the modulation index. Also the PVG terminal voltage remains close to the nominal voltage i.e. 2 kV.

However, for $\pm 4\%$ variation e.g. 4.8 kA to 5.2 kA, specifying same $V_{inv}-\phi_{inv}$ produces insignificant change as may be seen from a comparison of Table 3.5 and Table 3.6. So same $V_{inv}-\phi_{inv}$ specifications can be recommended only for a slight variation ($\pm 4\%$) in the available PVG current.

Table 3.5 Load flow solutions at a given load for change of PVG current without updating $V_{inv}-\phi_{inv}$ specifications for the inverter

Sl no.	I_{pho} (kA)	Specified V_{inv} (p.u.)	Specified ϕ_{inv} (deg)	m_a	PF_{inv}	P_{inv} (MW)	Q_{inv} (MVAR)	Total MW_{loss}	Total $MVAR_{loss}$
1	4	1.0230	-2.3955	0.6580	0.9875	9.5895	1.5328	10.4327	23.3558
2	4.8	1.0230	-2.3955	0.8027	0.9875	9.5895	1.5328	10.2655	23.3558
3	5	1.0230	-2.3955	0.8393	0.9875	9.5895	1.5328	10.2282	23.3558
4	5.2	1.0230	-2.3955	0.8758	0.9875	9.5895	1.5328	10.1950	23.3558
5	6	1.0230	-2.3955	1.0554	0.9875	9.5895	1.5328	10.0988	23.3558

Table 3.6 Load flow results at a given load for change of PVG current with the corresponding $V_{inv}-\phi_{inv}$ specifications for the inverter

Sl no.	I_{pho} (kA)	Specified V_{inv} (p.u.)	Specified ϕ_{inv} (deg)	m_a	PF_{inv}	P_{inv} (MW)	Q_{inv} (MVAR)	Total MW_{loss}	Total $MVAR_{loss}$
1	4	1.0226	-2.6791	0.8386	0.9825	7.5932	1.4386	10.2755	23.6441
2	4.8	1.0229	-2.4520	0.8391	0.9871	9.1902	1.4928	10.2372	23.4328
3	5	1.0230	-2.3955	0.8393	0.9875	9.5895	1.5328	10.2282	23.3558
4	5.2	1.0231	-2.3391	0.8395	0.9878	9.9883	1.5730	10.2194	23.2794
5	6	1.0234	-2.1126	0.8402	0.9902	11.5839	1.6312	10.1865	23.0845

3.3.4 Performance with Variation of System Load

The impact of using same control parameters ($V_{inv}-\phi_{inv}$) for the inverter was also analyzed for 5% to 25% decrease or increase in the day peak load of 405 MW at various available peak insolation. Tables 3.7 and 3.8 respectively shows the load flow records for a $I_{pho} = 5$ kA and 25 kA. The generation of the generator at the PVG interfacing bus i.e. gen no. 3 was decreased in proportion to the decrease in the load so that the available PVG capacity (I_{pho}) could be fully utilized and as a result slack generation also decreased. On the other hand, when the load was increased the available PVG capacity

was fully utilized while generation at bus no. 3 and slack generator increased to supply the remainder of the required generation. The a_1 and b_1 constants in equation 3.1 were found almost the same for 5% to 25% load variation as those for the base load of 405 MW so that the same $V_{inv}-\phi_{inv}$ could be specified for load variation of up to $\pm 25\%$ provided the corresponding PVG available capacity does not change. The inverter power factor and modulation index also remain within usual and acceptable range.

Table 3.7 Load flow results for the variation in load (Δ_{Load}) from the day peak of 405 MW while PVG current is 5 kA and $V_{inv} = 1.0230$ p.u., $\phi_{inv} = -2.3955^\circ$

Sl. no.	Δ_{Load} (%)	m_a	PF_{inv}	P_{inv} (MW)	Q_{inv} (MVAR)	P_{slack} (MW)	Q_{slack} (MVAR)	$P_{Gen\ 3}$ (MW)	$Q_{Gen\ 3}$ (MVAR)	Total MW_{loss}	Total $MVAR_{loss}$
1	-25	0.8280	0.9881	9.7147	1.5127	177.9516	76.5994	121.5225	63.0450	5.8607	5.5278
2	-20	0.8347	0.9877	9.6402	1.5246	187.3248	82.4482	133.2180	121.5225	6.5980	8.56014
3	-15	0.8393	0.9875	9.5894	1.5328	196.7375	88.3992	144.9135	133.2180	7.4013	11.8486
4	-10	0.8417	0.9873	9.5633	1.5370	206.1912	94.4564	156.6090	144.9135	8.2720	15.4033
5	-5	0.8417	0.9873	9.5629	1.5370	215.6874	100.6240	168.3045	156.6090	9.2133	19.2351
6	+5	0.8343	0.9877	9.6444	1.5240	234.8144	113.3110	191.6955	168.3045	11.3200	27.7783
7	+10	0.8267	0.9882	9.7290	1.5104	244.4490	119.8410	203.3910	191.6955	12.4923	32.5169
8	+15	0.8166	0.9887	9.8449	1.4919	254.1340	126.5030	215.0865	203.3910	13.7486	37.5873
9	+20	0.8037	0.9893	9.9940	1.4681	263.8719	133.3040	226.7820	215.0865	15.0958	43.0067
10	+25	0.7885	0.9902	10.1783	1.4387	273.6653	140.2520	238.4775	226.7820	16.5364	48.7945

Table 3.8 Load flow results for the variation in load (Δ_{Load}) from the day peak of 405 MW while PVG current is 25 kA and $V_{inv} = 1.0320$ p.u., $\phi_{inv} = 3.1520^\circ$

Sl. no.	Δ_{Load} (%)	m_a	PF_{inv}	P_{inv} (MW)	Q_{inv} (MVAR)	P_{slack} (MW)	Q_{slack} (MVAR)	$P_{Gen\ 3}$ (MW)	$Q_{Gen\ 3}$ (MVAR)	Total MW_{loss}	Total $MVAR_{loss}$
1	-25	0.8528	0.9945	49.8751	5.2537	137.7315	83.2208	121.5230	69.0576	6.0716	2.2783
2	-20	0.8555	0.9944	49.7167	5.2731	147.1880	88.8793	133.2180	76.4168	6.8108	5.2960
3	-15	0.8579	0.9944	49.5797	5.2898	156.6860	94.6379	144.9140	83.9306	7.6136	8.5685
4	-10	0.8599	0.9943	49.4651	5.3039	166.2271	100.5010	156.6090	91.6050	8.4823	12.1056
5	-5	0.8615	0.9943	49.3738	5.3151	175.8128	106.4720	168.3050	99.4465	9.4198	15.9182
6	+5	0.8634	0.9942	49.2660	5.3283	195.1257	118.7580	191.6960	115.6600	11.5129	24.4181
7	+10	0.8637	0.9942	49.2518	5.3300	204.8570	125.0840	203.3910	124.0490	12.6752	29.1323
8	+15	0.8634	0.9942	49.2662	5.3283	214.6413	131.5390	215.0870	132.6380	13.9197	34.1764
9	+20	0.8626	0.9942	49.3106	5.3228	224.4812	138.1300	226.7820	141.4370	15.2508	39.5674
10	+25	0.8613	0.9943	49.3870	5.3135	234.3796	144.8650	238.4780	150.4600	16.6731	45.3248

3.4 Performance Analysis under P_{inv} - Q_{inv} Control Mode of PVG Inverter Interfaced at a PV Bus in the 5-Bus System

The performance of the PVG interfaced at the PV bus was investigated under P_{inv} - Q_{inv} specifications mode of control for the inverter at different available currents from PVG. Table 3.9 shows the key results for load flow.

As mentioned in Sec. 2.3.1 P_{inv} was specified by multiplying the available I_{pho} by the nominal voltage of the PVG (2 kV in the specified system). Q_{inv} was considered 5%-7% of P_{inv} provided the $\sqrt{P_{inv}^2 + Q_{inv}^2}$ does not exceed the rated peak capacity of the PVG. However, Q_{inv} was also varied within 8% to 10% of P_{inv} that resulted in lower power factor.

Compared to the V_{inv} - ϕ_{inv} control, the mode of P_{inv} - Q_{inv} control does not involve any hassle to compute P_{inv} - Q_{inv} to be specified. However, for the same I_{pho} it results in less reactive power transfer to the grid while MW and MVAR losses are also slightly higher than those under V_{inv} - ϕ_{inv} control.

Table 3.9 Results for P_{inv} - Q_{inv} control mode of the inverter for the PVG interfaced at a PV bus (bus no. 3)

Sl no.	I_{pho} (kA)	Specified P_{inv} (MW)	Specified Q_{inv} (MVAR)	m_a	PF_{inv}	Total MW_{loss}	Total $MVAR_{loss}$	V_2 (p.u.)	V_4 (p.u.)
1	24	48	2.4	0.8402	0.9988	10.3153	22.7882	0.9604	0.9122
2	16	32	1.6	0.8313	0.9988	10.0520	22.5414	0.9603	0.9124
3	10	20	1	0.8212	0.9988	10.0739	23.2126	0.9602	0.9124
4	5	10	0.5	0.8006	0.9988	10.2499	24.3457	0.9600	0.9124
5	1	2	0.1	0.6030	0.9988	10.8005	25.6353	0.9598	0.9123

Table 3.10 shows the load flow output for a $I_{pho} = 24$ kA using same P_{inv} - Q_{inv} specifications for 5% to 25% decrease or increase in the day peak load of 405 MW. It is evident that the same P_{inv} - Q_{inv} could be specified for load variation of up to $\pm 25\%$ provided the corresponding PVG available capacity does not change and has been utilized fully as mentioned in section 3.3.4.

Table 3.10 Load flow results for the variation in load (Δ_{Load}) from the day peak of 405 MW while PVG current is 24 kA and $P_{inv} = 48$ MW, $Q_{inv} = 2.4$ MVAR

Sl. no.	Δ_{Load} (%)	m_a	PF_{inv}	P_{inv} (MW)	Q_{inv} (MVAR)	P_{slack} (MW)	Q_{slack} (MVAR)	$P_{Gen\ 3}$ (MW)	$Q_{Gen\ 3}$ (MVAR)	Total MW_{loss}	Total $MVAR_{loss}$
1	-25	0.8424	0.9988	48.00	2.40	139.5685	82.8664	121.5225	72.0563	6.0140	4.9228
2	-20	0.8424	0.9988	48.00	2.40	148.8693	88.5626	133.2180	79.4128	6.7603	7.9755
3	-15	0.8424	0.9988	48.00	2.40	158.2326	94.3539	144.9135	86.9243	7.5692	11.2783
4	-10	0.8424	0.9988	48.00	2.40	167.6610	100.2441	156.6091	94.5965	8.4431	14.8408
5	-5	0.8424	0.9988	48.00	2.40	177.1569	106.2378	168.3046	102.4355	9.3846	18.6736
6	+5	0.8424	0.9988	48.00	2.40	196.3637	118.5547	191.6955	118.6422	11.4823	27.1970
7	+10	0.8424	0.9988	48.00	2.40	206.0810	124.8887	203.3910	127.0252	12.6450	31.9138
8	+15	0.8424	0.9988	48.00	2.40	215.8791	131.3476	215.0865	135.6063	13.8886	36.9539
9	+20	0.8424	0.9988	48.00	2.40	225.7623	137.9384	226.7820	144.3958	15.2174	42.3342
10	+25	0.8424	0.9988	48.00	2.40	235.7354	144.6686	238.4775	153.4047	16.6359	48.0733

3.5 Performance Analysis of PVG Interfaced at a PQ Bus in the 5-Bus System

PQ bus is referred to as a load bus at which active power and reactive power are specified. Owing to the uncontrolled voltage magnitude and angle of a PQ bus $V_{inv}-\phi_{inv}$ control mode is not feasible for the inverter of a PVG interfaced at a PQ bus. Only $P_{inv}-Q_{inv}$ control mode of PWM inverter is suitable.

Figure 3.12 shows the one-line diagram of a PVG interfaced at a PQ bus (bus no. 4) of the 5 bus test system.

The method to specify the values for the $P_{inv}-Q_{inv}$ control mode of the PWM inverter is same as that for the $P_{inv}-Q_{inv}$ control when the PVG is interfaced at the PV bus as mentioned in Sec. 3.4. Table 3.11 shows the results for the various available PVG currents. It is evident that the voltage magnitudes of the interfaced PQ bus (bus 4) and the neighbouring PQ bus (bus 5) show significant improvement with increase in the available PVG current compared to the cases where PVG was not interfaced and interfaced at a PV bus.

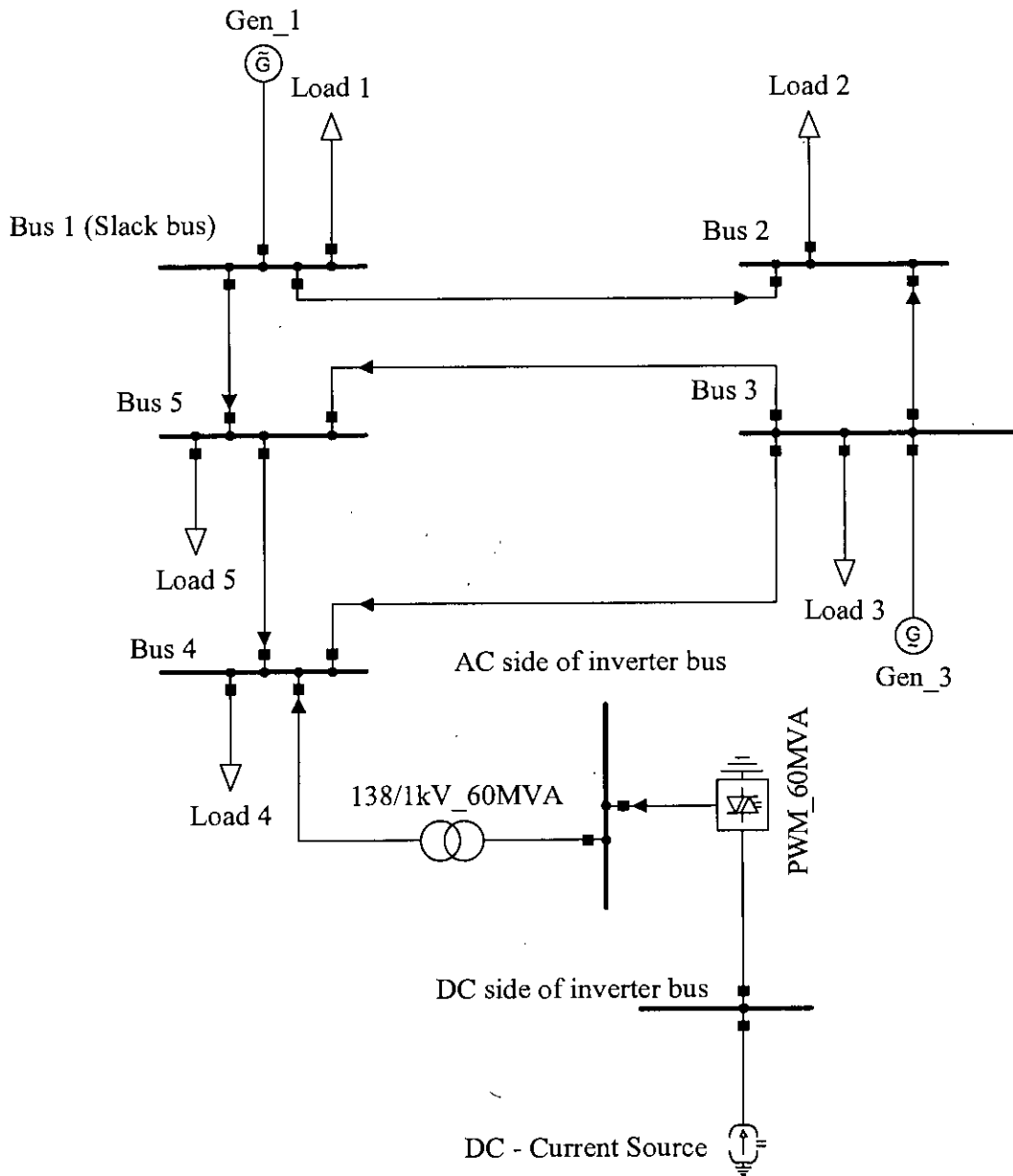


Figure 3.12 One line diagram of a 5-bus power system where PVG is interfaced at a PQ bus

MW and MVAR losses of the system decrease reasonably and become less than the losses before interfacing the PVG. On the other hand, when the PVG was interfaced at a PV bus under $V_{inv}-\phi_{inv}$ control, MW and MVAR losses (Table 3.4) decreased with PVG current but the MW loss was not less than that before interfacing the PVG.

It is also observed that the modulation index (m_a) of the inverter remains lower than the case when PVG was interfaced at a PV bus.

It should be noted that if the set of equations (2.8), (2.9), (2.10) and (2.11) is applied in the same way as that done for PV bus to exercise $V_{inv}-\phi_{inv}$ control mode for the PVG interfaced at a PQ bus, unique values of the constants of the equations i.e. a_2 , b_2 , a_3 and b_3 cannot be obtained. In other words the constants determination process for $V_{inv}-\phi_{inv}$ control mode using a test set of injections from the PVG requires an arbitrary choice of the constants in case of a PQ bus.

It was also observed through simulations that $P_{inv}-Q_{inv}$ specification for a given I_{ph0} remains valid for $\pm 25\%$ variation in the system load as in the case for interfacing PVG with a PV bus under $P_{inv}-Q_{inv}$ control.

“At a glance” comparison of voltage profiles and MW losses for interfacing a PVG at a PV and at a PQ bus has been shown in Figure 3.13 and Figure 3.14 respectively. From the comparisons it is evident that interfacing a PVG at a PQ bus is preferable when there is an option to interface it either at a PQ bus or at a PV bus.

Table 3.11 Load flow results for various available currents for the PVG interfaced at a PQ bus (Bus No. 4) of the 5 bus test system and P_{inv} - Q_{inv} control mode of inverter

Sl no.	I_{pho} (kA)	Specified P_{inv} (MW)	Specified Q_{inv} (MVAR)	V_{inv} (p.u.)	ϕ_{inv} (deg)	m_a	PF_{inv}	P_{slack} (MW)	Q_{slack} (MVAR)	P_3 (MW)	Q_3 (MVAR)	Total MW_{loss}	Total $MVAR_{loss}$
1	2	3	4	5	6	7	8	9	10	11	12	13	14
1	24	48	2.4	0.9531	-0.7519	0.7825	0.9988	183.5640	105.4063	180	104.6619	7.2811	10.0682
2	16	32	1.6	0.9422	-4.0176	0.7656	0.9988	200.2137	104.6741	180	108.4018	7.6617	11.0970
3	10	20	1	0.9323	-6.5281	0.7488	0.9988	213.0338	104.6913	180	112.0882	8.5084	16.7795
4	5	10	0.5	0.9229	-8.6732	0.7234	0.9988	223.9535	105.1050	180	115.7862	9.4045	20.8912
5	1	2	0.1	0.9145	-10.4321	0.5405	0.9988	232.8568	105.7168	180	119.1885	10.6214	24.9054

Table 3.11 (extended)

Sl no.	I_{pho} (kA)	V_2 (p.u.) 15	ϕ_2 (deg) 16	V_3 (p.u.) 17	ϕ_3 (deg) 18	V_4 (p.u.) 19	ϕ_4 (deg) 20	V_5 (p.u.) 21	ϕ_5 (deg) 22
1	24	0.9603	-4.5884	1.02	-0.6934	0.9435	-3.7432	0.9742	-3.6788
2	16	0.9602	-5.1479	1.02	-1.6794	0.9355	-6.0517	0.9716	-4.4808
3	10	0.9601	-5.5795	1.02	-2.4392	0.9280	-7.8231	0.9691	-5.0939
4	5	0.9600	-5.9481	1.02	-3.0875	0.9206	-9.3325	0.9667	-5.6135
5	1	0.9598	-6.2496	1.02	-3.6173	0.9140	-10.5661	0.9645	-6.0356

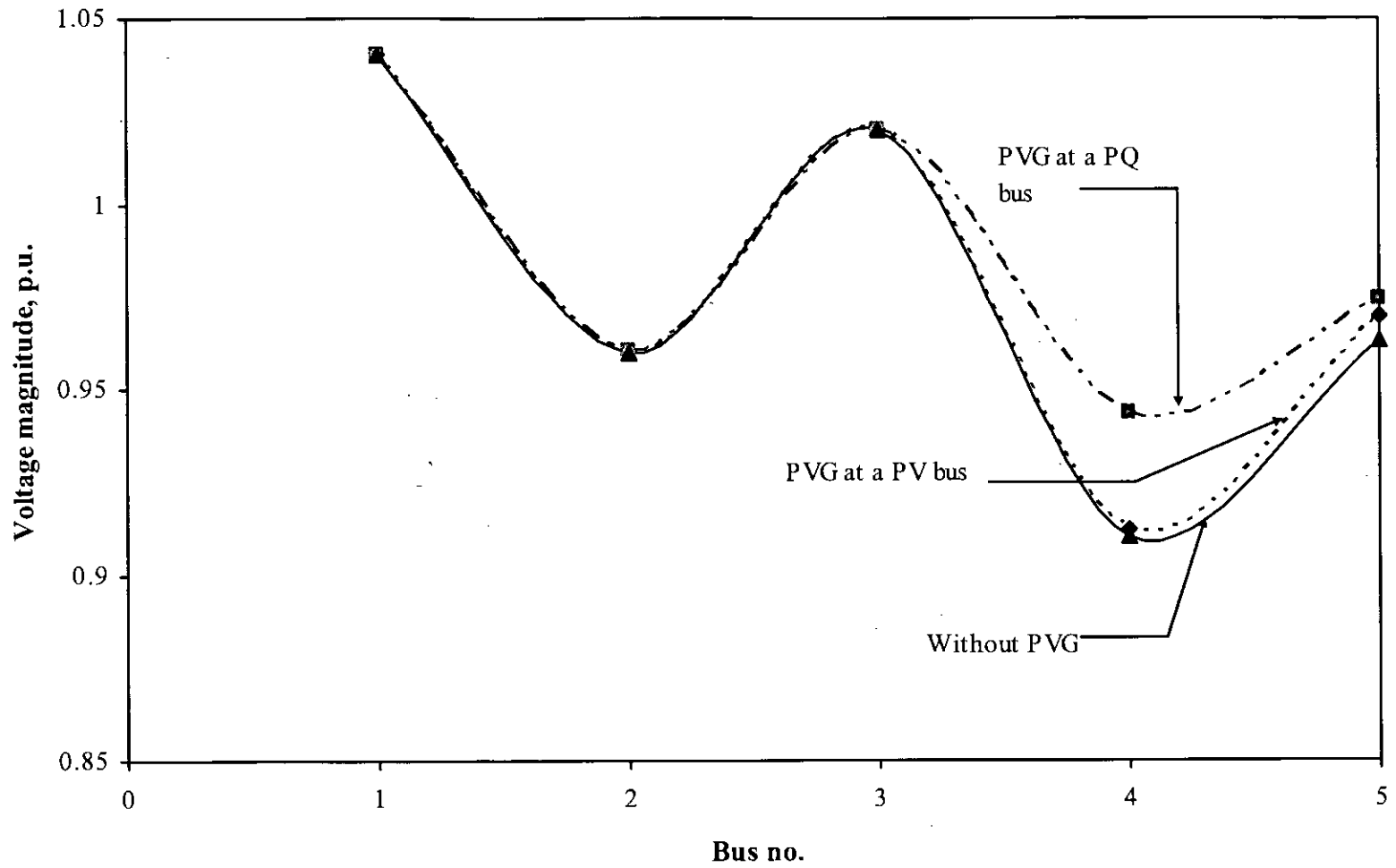


Figure 3.13 Voltage profile for all buses with PVG at a PQ and at a PV bus in the 5-bus test system

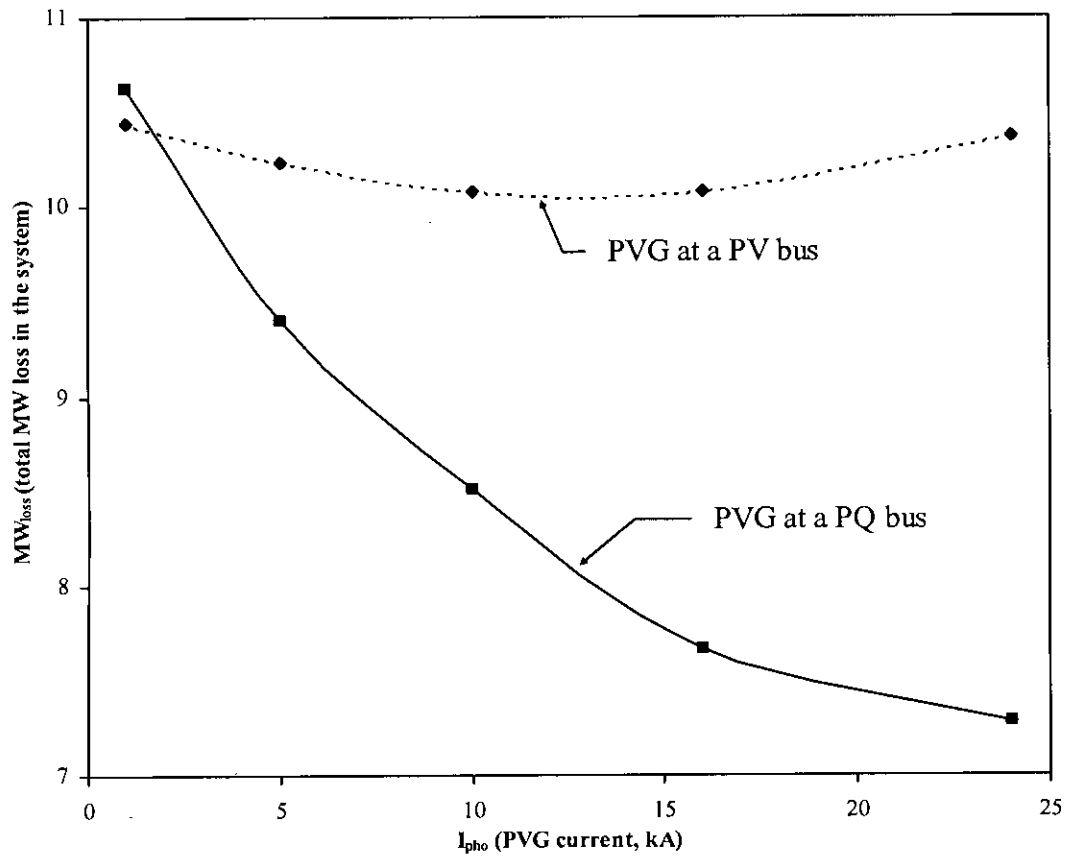


Figure 3.14 MW loss in the system when PVG is interfaced at a PQ bus and at a PV bus

3.6 Performance Analysis for 14-bus System with Embedded PVG

Figure 3.15 shows the single line diagram of a 14 bus 138 kV power system [9] with an installed capacity 1100MW and a day peak load of about 780 MW. Base values for the system is 100 MVA. Appendix-A.3 and A.4 give system data.

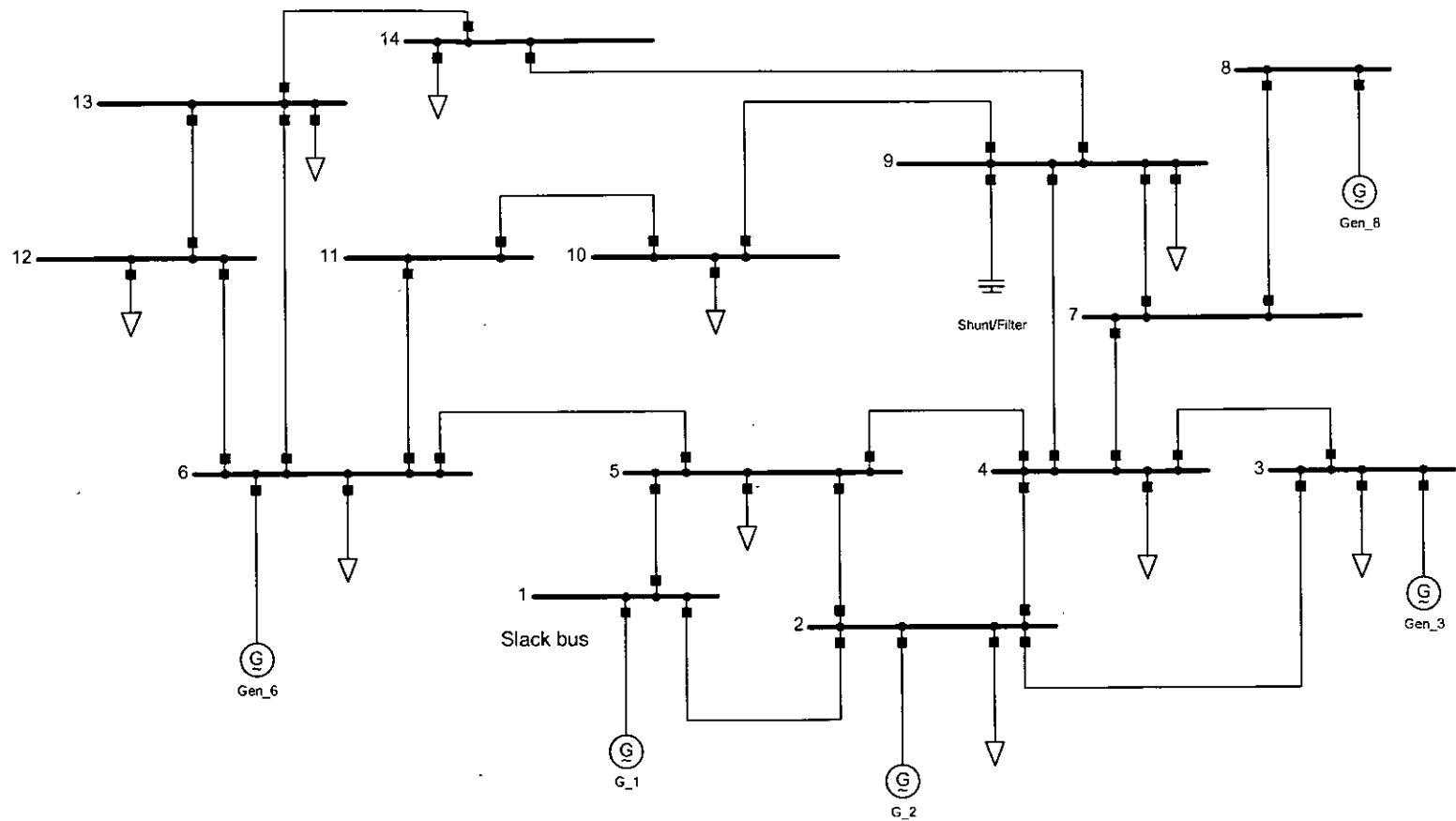


Figure 3.15 One line diagram of a 14 bus power system

The PVG is considered to be of 50 MW peak capacity with a nominal voltage of 2 kV and interfaced through a 60 MVA PWM inverter and a 60 MVA of transformer. As mentioned in Sec. 3.3 and 3.4 either $V_{inv}-\varphi_{inv}$ or $P_{inv}-Q_{inv}$ control mode is applicable for the operation of the PWM inverter when interfaced with a PV bus. For interfacing with a PQ bus only $P_{inv}-Q_{inv}$ control mode is applicable.

For $V_{inv}-\varphi_{inv}$ control mode when the PVG is interfaced at the bus no. 6 (PV bus), specified values of $V_{inv}-\varphi_{inv}$ were computed using the following set of four equations.

$$\varphi_{PV} = a_1 P_{inject} + b_1 \quad (2.8)$$

$$V_{inv} = a_2 \Delta I_{pho} + b_2; \quad I_{pho} > 0 \quad (2.9)$$

$$\vartheta = a_3 \Delta I_{pho} + b_3 \quad (2.10)$$

$$\varphi_{inv} = \varphi_{PV} + \vartheta \quad (2.11)$$

The constants have been determined to be as follows using the procedures mentioned in Sec. 3.3.

$$a_1 = 0.1401, b_1 = -13.3929$$

$$a_2 = -4.5 \times 10^{-4}, b_2 = 1.0820, a_3 = 0.0960, b_3 = 2.5989.$$

Table 3.12 shows the key results for $V_{inv}-\varphi_{inv}$ control after interfacing the PVG at bus no. 6 of the 14 bus system. It is observed that both modulation index and power factor of the inverter increase with available PVG current. Since the PVG has been modeled by an ideal DC current source that can not consider the power output limit of a PVG at a given insolation due to DIGSILENT limitations, the simulations at lower available PVG currents (7 kA and less) show that nominal PVG output voltage (DC bus

voltage) can not be maintained rather the voltage rises abnormally being accompanied with a drastic fall in the modulation index.

Table 3.12 Load flow results for variations in available current from the PVG interfaced at a PV bus (bus no. 6) of the 14 bus test system and $V_{inv}-\phi_{inv}$ control mode of inverter

Sl No.	I_{pho} (kA)	Specified V_{inv} (p.u.)	Specified ϕ_{inv} (deg)	m_a	PF_{inv}	P_{inv} (MW)	Q_{inv} (MVAR)	Total MW_{loss}	Total $MVAR_{loss}$	Voltage of the inverter's DC side V_{DC} (kV)
1	24	1.0815	-4.5105	0.8958	0.9933	47.5080	5.5079	23.8380	102.8734	2.0030
2	16	1.0779	-7.4570	0.8879	0.9931	31.5640	3.7100	24.3649	107.8486	2.0023
3	10	1.0752	-9.6889	0.8815	0.9915	19.6166	2.5669	24.9790	112.5535	2.0044
4	9	1.0748	-9.9990	0.8633	0.9917	17.9613	2.3284	25.0951	113.3670	2.0447
5	8	1.0743	-10.3980	0.8670	0.9912	15.8387	2.1106	25.2243	114.3510	2.0338
6	7	1.0739	-10.8000	0.8728	0.9894	13.7092	2.0069	25.3584	115.2570	2.0186
7	6	1.0734	-10.7990	0.7399	0.9943	13.6889	1.4650	25.5174	115.8060	2.3780
8	5	1.0730	-10.8990	0.6307	0.9964	13.1445	1.1148	25.7650	116.3660	2.7867
9	1	1.0713	-13.0040	0.2486	0.8905	2.0749	0.9544	32.2266	121.2893	7.0449

The effect of using same $V_{inv}-\phi_{inv}$ when the insolation change was analyzed. It was found to produce insignificant change for up to $\pm 4\%$ variation in the insolation for a given load.

The impact of embedding the PVG at the same bus has also been analyzed considering $P_{inv}-Q_{inv}$ control of the inverter. As in Sec. 3.4 for $P_{inv}-Q_{inv}$ control mode, the specified P_{inv} is calculated multiplying available PVG current and nominal voltage of the PVG while specified value Q_{inv} is computed taking 5%-7% of P_{inv} . As mentioned before computations for the $P_{inv}-Q_{inv}$ control mode is easier than for the $V_{inv}-\phi_{inv}$ control

mode. Compared to the $V_{inv}-\phi_{inv}$ control, the MW loss is less in general and the DC bus voltage can be maintained close to the nominal value ($V_{nom-pho}$) for the PVG current up to 4 kA through $P_{inv}-Q_{inv}$ control as shown in Table 3.13.

Table 3.13 Load flow results for variations in available current from the PVG interfaced at a PV bus (bus no. 6) of the 14 bus test system and $P_{inv}-Q_{inv}$ control mode of inverter

Sl no.	I_{pho} (kA)	Speci- fied P_{inv} (MW)	Speci- fied Q_{inv} (MVAR)	V_{inv} (p.u.)	ϕ_{inv} (deg)	m_a	PF_{inv}	Total MW_{loss}	Total $MVAR_{loss}$	Votage of the inverter's DC side V_{DC} (kV)
1	24	48	2.4	1.0787	-4.3874	0.8798	0.9987	23.8325	105.9002	2.024
2	16	32	1.6	1.0760	-7.3551	0.8711	0.9987	24.3557	109.8412	2.0304
3	10	20	1	1.0738	-9.6022	0.8608	0.9987	24.9715	113.9860	2.0447
4	5	10	0.5	1.0719	-11.4901	0.8395	0.9987	25.6455	118.2398	2.0887
5	4.5	9	0.45	1.0717	-11.6800	0.8350	0.9987	25.7230	118.7058	2.0992
6	4	8	0.4	1.0715	-11.8690	0.8293	0.9987	25.8032	119.1794	2.1127
7	3	6	0.3	1.0712	-12.2490	0.8122	0.9987	25.9746	120.1489	2.1557
8	2	4	0.2	1.0708	-12.6300	0.7760	0.9987	26.1769	121.1485	2.2547
9	1	2	0.1	1.0704	-13.0111	0.6324	0.9987	26.5969	122.1783	2.7645

The effect of load variation up to $\pm 25\%$ from the day peak load 780 MW when insolation remains unchanged has been analyzed with and without updating $V_{inv}-\phi_{inv}$ corresponding to available PVG current of 10 kA. It was observed that updating $V_{inv}-\phi_{inv}$ does not produce significant difference in the output results for a load variations of up to $\pm 25\%$. This was also valid for $P_{inv}-Q_{inv}$ mode of control i.e. updating $P_{inv}-Q_{inv}$ is not required so long the load change within $\pm 25\%$ at a given insolation.

Following three additional cases have also been analyzed through load flow analysis using P_{inv} - Q_{inv} control mode.

1. A PVG interfaced with a PQ bus
2. Two PVGs interfaced with a PV and a PQ bus concurrently
(one at each bus)
3. Two PVGs interfaced with two different PQ buses
concurrently (one at each bus)

Table 3.14 compares one of the key performance e.g. MW losses of the system for the three cases with P_{inv} - Q_{inv} control and that before embedding a PVG. Figure 3.16 compares the system voltage profile before and after interfacing the PVG for all the cases and show better profile for embedding PVGs at PQ buses. Also it is worth noting that embedding higher number of PVGs can reduce the system loss more.

Table 3.14 MW loss in the 14 bus system before and after interfacing the PVG in four cases with P_{inv} - Q_{inv} control mode of the inverter

SI no.	I_{pho} (kA)	PVG at a PQ bus		Two PVGs at a PV and a PQ bus concurrently			Two PVGs at two different PQ buses concurrently			Before PVG
		V_{DC} (kV)	Total MW_{loss}	V_{DC} (PVG at bus no. 6)	V_{DC} (PVG at bus no. 12)	Total MW_{loss}	V_{DC} (PVG at bus no. 12)	V_{DC} (PVG at bus no. 14)	Total MW_{loss}	Total MW_{loss}
1	24	2.0241	27.0437	2.0240	2.0241	24.2407	2.02404	2.02564	17.3064	26.1382
2	16	2.0306	26.7640	2.0304	2.0306	24.2311	2.0306	2.0317	18.4247	
3	10	2.0449	26.6267	2.0447	2.0449	24.7978	2.0449	2.0457	20.5503	
4	5	2.0888	26.5604	2.0887	2.0888	25.6726	2.0888	2.0893	23.2629	

It should be noted that the load flow analysis converged in 4 iterations before and after interfacing the PVG.

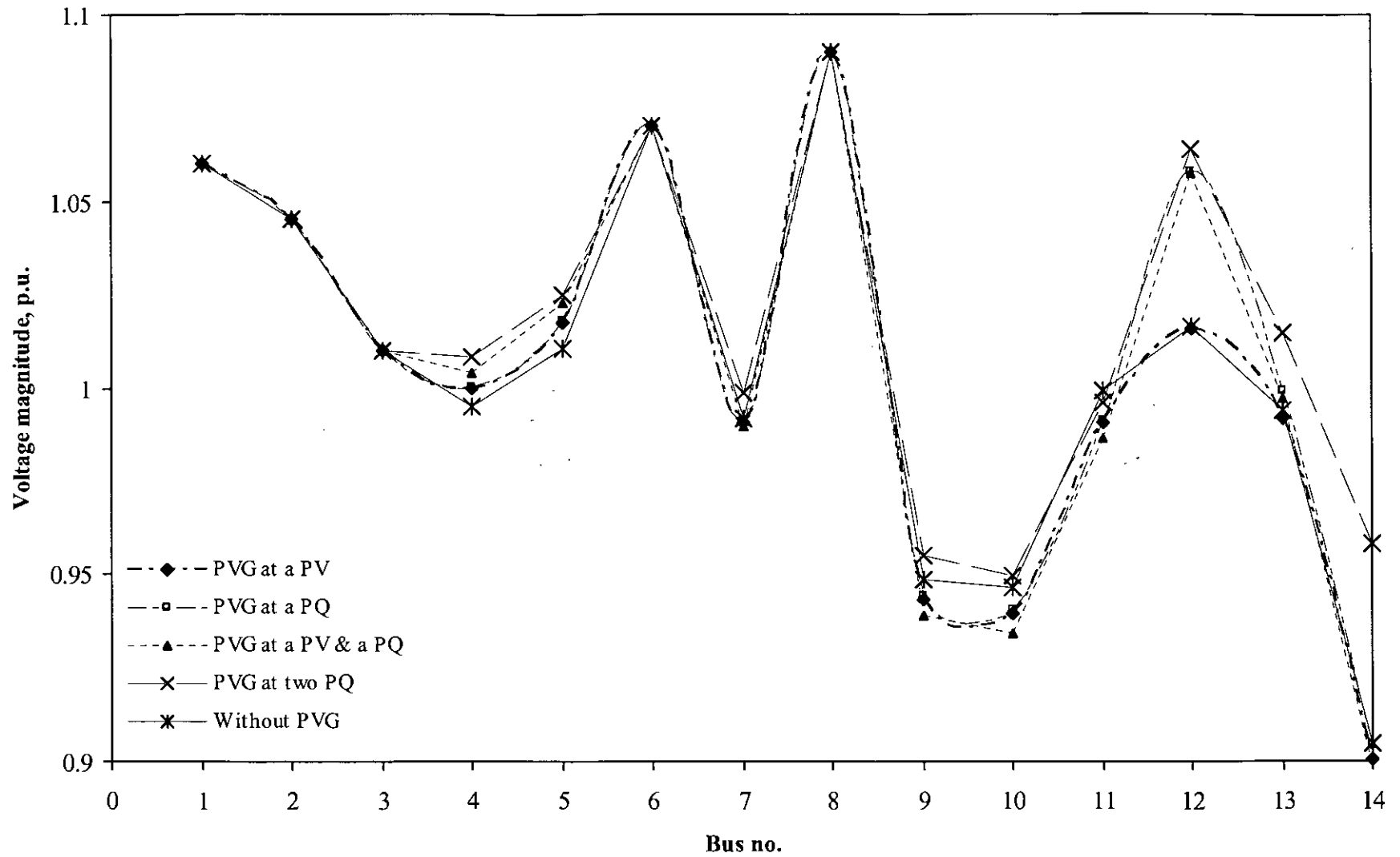


Figure 3.16 shows the voltage profile at all buses in the 14-bus test system before and after interfacing the PVG for four cases with P_{inv} - Q_{inv} control mode of the inverter

3.7 Analysis of Total Harmonic Distortion (THD) due to an Embedded PVG

The output voltage of an inverter is not a perfect sine wave and contains harmonics i.e. multiples of fundamental frequency f_1 . For a PWM inverter the percentage of the fundamental components in terms of the input DC voltage is always a linear function of the amplitude modulation ratio m_a if $m_a \leq 1.0$.

$$m_a = \frac{\hat{V}_{\text{control}}}{\hat{V}_{\text{tri}}} \quad (3.5)$$

where,

m_a is the amplitude modulation ratio and for linear modulation $m_a \leq 1.0$

\hat{V}_{control} is the peak amplitude of the control or modulating signal

\hat{V}_{tri} is the amplitude of the triangular or carrier signal

$$(\hat{V}_{\text{AN}})_1 = m_a \left(\frac{V_{\text{DC}}}{2} \right) \quad (3.6)$$

where,

$(\hat{V}_{\text{AN}})_1$ is the peak amplitude of the fundamental frequency component

V_{DC} is the input voltage of the inverter i.e. the DC bus voltage which is also equal to the output nominal voltage ($V_{\text{nom-pho}}$) of the PVG interfaced with the grid through the inverter

Equation (3.6) can be expressed in terms of the line-to-line voltage as,

$$\begin{aligned}
 (V_{LL})_1 &= \frac{\sqrt{3}}{\sqrt{2}} (\hat{V}_{AN})_1 \\
 &= \frac{\sqrt{3}}{\sqrt{2}} m_a \left(\frac{V_{DC}}{2} \right) \\
 \text{or } \frac{(V_{LL})_1}{V_{DC}} &= 0.612 m_a \tag{3.7}
 \end{aligned}$$

where,

$(V_{LL})_1$ is the line-to-line rms voltage of the fundamental frequency

As for instance,

$$\text{for } m_a = 0.8, \frac{(V_{LL})_1}{V_{DC}} = 0.49$$

In a work [2] the typical frequency spectrum of a PWM inverter output voltage waveform has been analyzed to determine the order of harmonics present as in equation (3.8) and their ratio to the input DC voltage at a given modulation index m_a as in Table 3.15. It should be noted that while the fundamental component is a linear function of m_a (for $m_a \leq 1.0$) the harmonics amplitudes do not vary linearly with m_a .

$$h = j m_f \pm k \tag{3.8}$$

where,

h is the order of harmonics excluding 3 or multiple of 3 for the line-to-line voltage,

values of parameters j and k are related as follows in their usual range

j	1	2	3	4
k	2,4	1,5	2,4	1,5,7

frequency modulation ratio, $m_f = \frac{f_s}{f_1}$,

when f_s is the carrier or triangular wave frequency, and

f_1 is the fundamental frequency

The value m_f is usually an odd integer >9 and typically equal to 39 i.e. $f_s = 1.95$ kHz so that the switching loss is not much and audible noise is not produced being outside the 6 kHz to 20 kHz range.

Table 3.15 Harmonic order and corresponding values of $\frac{(V_{LL})_h}{V_{DC}}$ for $m_a=0.8$ and $m_f=39$

Harmonic order h	Line-to-line harmonic voltage as a ratio of input DC voltage $\frac{(V_{LL})_h}{V_{DC}}$
35	0.005
37	0.135
41	0.135
43	0.005
73	0.008
77	0.192
79	0.192
83	0.008
113	0.064
115	0.108
119	0.108
121	0.064
149	0.010
151	0.051
155	0.064
157	0.064
161	0.051
163	0.010

Using the value of h and corresponding $\frac{(V_{LL})_h}{V_{DC}}$, $m_a=0.8$ and equation (3.7) the

equation (3.9) can be obtained.

$$\frac{(V_{LL})_h}{(V_{LL})_1} = \frac{(V_{LL})_h}{0.49 V_{DC}} \quad (3.9)$$

Using the equation 3.9 and the ratios of $\frac{(V_{LL})_h}{V_{DC}}$ in the Table 3.15 the line-to-

line harmonic voltage magnitudes have been calculated in this work as in Table 3.16 as percentage of the inverter fundamental output voltage magnitude.

Table 3.16 Percentage values of the harmonic voltage magnitudes in terms of fundamental frequency output voltage

Harmonic order h	Harmonic voltage magnitude in % of inverter fundamental output voltage magnitude
	$\frac{(V_{LL})_h}{(V_{LL})_1}$
35	1.02
37	27.55
41	27.55
43	1.02
73	1.00
77	23.98
79	23.98
83	1.00
113	7.99
115	13.49
119	13.49
121	7.99
149	1.25
151	6.37
155	7.99
157	7.99
161	6.37
163	1.25

The harmonics as percentage of the fundamental obtained in Table 3.16 have been specified as input data for doing a harmonic power flow analysis using the DIGSILENT 13.0. Then the THD is obtained.

For the 5-bus test system the case of interfacing a PVG with a PV bus under $V_{inv}-\phi_{inv}$ or $P_{inv}-Q_{inv}$ control was analyzed for THDs at different available PVG currents. THDs at all the grid buses for $I_{pho}=1$ kA and 24 kA are shown in Table 3.17 as the representative cases. Notably the THD analysis is found almost the same for $V_{inv}-\phi_{inv}$ or $P_{inv}-Q_{inv}$ control mode. It was observed that the THD at a bus decrease with increase in the distance from the AC side of the inverter bus and shows slightly higher value for the higher available PVG current. The THD at the inverter AC bus, the grid system bus 3 at which the PVG was considered interfaced and at its neighbouring buses (bus 1 and bus 2) exceeded the IEEE standard 519 limit [10] i.e. 2.5% for 138 kV system. This suggests the need of an appropriate filter at the inverter AC bus.

Notably use of higher switching frequency [2] outside the range of audible noise i.e. $f_s < 6$ kHz or $f_s > 20$ kHz may also make the filtering of harmonic easier though the switching loss will increase.

Table 3.17 Voltage THD for all the buses while the PVG is interfaced at a PV bus (bus 3) of the 5-bus test system corresponding to harmonic generated as in Table 3.16

Sl. No.	I_{pho} (kA)	Voltage THD in % of system voltage					
		Bus 1	Bus 2	Bus 3	Bus 4	Bus 5	AC bus of inverter
1	1	7.57	18.78	23.97	1.77	1.55	58.98
2	24	7.63	18.92	24.15	1.78	1.56	58.98

The THD in case of interfacing a PVG with a PQ bus through the PWM inverter in the 5-bus test system has been analyzed for different available PVG currents and shown for all the system (grid) buses for 1 kA and 24 kA in Table 3.18. It was observed that the THD at the inverter AC bus and only at bus 4 where the PVG was considered interfaced exceeded the IEEE standard limit i.e. 2.5% for 138 kV system. So it is evident that the PWM inverter gives less distortion and affects THDs at less number of buses when the PVG is interfaced at a PQ bus than at a PV bus.

Table 3.18 Voltage THD for all the buses while the PVG is interfaced at a PQ bus (bus 4) of the 5-bus test system corresponding to harmonic generated as in Table 3.16

Sl. No.	I _{pho} (kA)	Voltage THD in % of system voltage					
		Bus 1	Bus 2	Bus 3	Bus 4	Bus 5	AC bus of inverter
1	1	0.22	1.23	1.10	12.25	1.17	58.98
2	24	0.22	1.27	1.14	12.32	1.20	58.98

Also noteworthy is that like PVG at a PV bus, an appropriately designed filter at the inverter bus can reduce harmonics so that the high THD at the interfacing bus will come down to the IEEE limit as approved in the case of a PVG interfaced at a PQ bus.

3.8 Summary of Operating Strategies for PVG Embedded Power System

Based on extensive simulations on two test systems of different characteristics viz. a 5 bus and a 14 bus system the salient operating strategies may be formulated as follows

- 106085
- 1) The PWM inverter that interfaces the PVG at a PV bus can be controlled using $V_{inv-\phi_{inv}}$ or $P_{inv-Q_{inv}}$ control mode.
 - 2) The $V_{inv-\phi_{inv}}$ to be specified are computed using a pre determined set of 4 simple algebraic equations in a trivial time that require knowledge of peak (I_{pk} i.e. rated) and available (I_{pho}) photovoltaic current, and nominal voltage of a PVG i.e. $V_{nom-pho}$ which is the inverter DC side bus voltage V_{DC} .
 - 3) The $V_{inv-\phi_{inv}}$ specified under the day peak load remains valid up to $\pm 25\%$ variation in the load for a given I_{pho} provided the corresponding PVG capacity has been fully utilized.
 - 4) The $V_{inv-\phi_{inv}}$ specified for a given I_{pho} can also be used if I_{pho} varies by $\pm 4\%$ provided the system load does not change. Beyond this range, the PWM inverter's modulation index will exceed unity if $V_{inv-\phi_{inv}}$ are not updated and the DC bus voltage can not be maintained at the nominal value.
 - 5) Compared to $V_{inv-\phi_{inv}}$ control, $P_{inv-Q_{inv}}$ specification is easier. This requires setting P_{inv} as the product of available I_{pho} and nominal voltage $V_{nom-pho}$. The Q_{inv} is set as 5% to 7% of P_{inv} to achieve near unity power factor of the inverter. The specification of $P_{inv-Q_{inv}}$ for a given I_{pho} remains valid for $\pm 25\%$ variation in system load like $V_{inv-\phi_{inv}}$. However, for a variation in I_{pho} , $P_{inv-Q_{inv}}$ can easily be respecified.
 - 6) The PWM inverter that interfaces a PVG at PQ bus can be controlled using only $P_{inv-Q_{inv}}$ control mode. In this case also $P_{inv-Q_{inv}}$ updating is not essential unless the load varies beyond $\pm 25\%$.
 - 7) In general embedding a PVG at a PQ bus provides better performances than when embedded at a PV bus. Also the more the number of PVGs embedded the better will be the system performances.

- 8) The PWM inverter should preferably be operated in linear modulation range ($m_a \leq 1.0$). Because this will provide a PWM output and the fundamental frequency component of inverter output voltage will vary almost proportionately with the modulation index. However appropriate filter needs to be used to reduce THD at various system buses to the acceptable limit regardless of the value of the modulation index.

Chapter 4

Conclusion

4.1 Conclusion

Operating strategies for a PVG embedded in a large high voltage system has not been investigated into adequately till now. In this work this has been attempted. Due to be fewer harmonic, easier control and smaller switching losses PVG is interfaced using the pulse width modulated (PWM) inverter. Based on extensive load flow analysis of two test systems of different characteristics viz. a 138 kV 5-bus system (day peak 400 MW) and a 138 kV 14-bus system (day peak 780 MW) the salient operating strategies can be formulated as follows

- i) PVG can be interfaced at any PV or PQ bus of the system.
- ii) For the interfacing of the PVG at a PV bus the PWM inverter can be controlled using V_{inv} - ϕ_{inv} or P_{inv} - Q_{inv} control mode.
- iii) The specified values of V_{inv} and ϕ_{inv} has been computed using a pre determined set of 4 simple algebraic equations in a trivial time for the available solar insolation where knowledge of peak (I_{pk} i.e. rated) and available (I_{pho}) photovoltaic current, and nominal voltage of a PVG i.e. $V_{nom-pho}$ which is the inverter DC side bus voltage . These quantities can always be monitored from a single photovoltaic cell installed at the same site and then extending those for the number of cells in series and parallel paths in the PVG.

- iv) The $V_{inv-\phi_{inv}}$ specified under the day peak load remains valid up to $\pm 25\%$ variation in the load for a given I_{pho} provided the corresponding PVG capacity has been fully utilized.
- v) The $V_{inv-\phi_{inv}}$ specified for a given I_{pho} can also be used if I_{pho} varies by $\pm 4\%$ provided the system load does not change. Beyond this range, the PWM inverter's modulation index will exceed unity if $V_{inv-\phi_{inv}}$ are not updated and the DC bus voltage can not be maintained at the nominal value.
- vi) Compared to $V_{inv-\phi_{inv}}$ control, $P_{inv}-Q_{inv}$ specification is easier. This requires setting P_{inv} as the product of available I_{pho} and nominal voltage $V_{nom-pho}$. The Q_{inv} is set as 5% to 7% of P_{inv} to achieve near unity power factor of the inverter. The specification of $P_{inv}-Q_{inv}$ for a given I_{pho} remains valid for $\pm 25\%$ variation in system load like $V_{inv-\phi_{inv}}$. However, for a variation in I_{pho} , $P_{inv}-Q_{inv}$ can easily be respecified.
- vii) The PWM inverter that interfaces a PVG at PQ bus can be controlled using only $P_{inv}-Q_{inv}$ control mode. In this case also $P_{inv}-Q_{inv}$ updating is not essential unless the load varies beyond $\pm 25\%$.
- viii) In general embedding a PVG at a PQ bus provides better performances than when embedded at a PV bus. Also the more the number of PVGs embedded the better will be the system performances.
- ix) The PWM inverter should preferably be operated in linear modulation range ($m_a \leq 1.0$). Because this will provide a PWM output and the fundamental frequency component of inverter output voltage will vary almost proportionately with the modulation index. However appropriate filter needs to be used to reduce THD at various system buses to the acceptable limit regardless of the value of the modulation index.

4.2 Recommendations for Further Research

The following points are worthy of further investigations.

- a) The proposed operating strategies can be implemented developing an experimental prototype.
- b) The results of simulation studies can be applied in the practical generation and load dispatch and security analysis of a grid system in which one or more PVGs are embedded.

References

1. Hu C. and White R. M., "Solar Cells from Basic to Advanced System", McGraw-Hill Book Co., New York, 1983.
2. Mohan N., Undeland T. M. and Robins W. P., "Power Electronics", John Wiley & Sons, Singapore, 2003.
3. Martin-Bucher, "Solar park Pocking (Bavaria, Germany)", Available on-line: www.martin-bucher.de/mb/10-1-pocking.html
4. "154MW Victorian Project", Available on-line: www.solarsystems.com.au/154MWVictorianProject.html
5. Tan Y. T., Kirschen D. S. and Jenkins N., "A Model of PV Generation Suitable for Stability", IEEE Trans. Energy Conversion, Vol. 19, No. 4, December 2004, pp. 748-755.
6. Lu B. and Shahidehpour M., "Short-Term Scheduling of Battery in a Grid-Connected PV/Battery System", IEEE Trans. Power System, Vol. 20, No. 2, May 2005, pp. 1053-1061.
7. Wood A. J. and Wollenberg B. F., "Power Generation, Operation and Control", John Wiley & Sons, New York, 1996.
8. Stevenson W.D., "Elements of Power System Analysis", McGraw-Hill Book Co., Singapore, 1982.
9. Pai M. A., "Computer Techniques in Power System Analysis", Tata McGraw-Hill Publishing Company Limited, New Delhi, 1986.
10. Burke J. J., "Power distribution engineering: fundamentals and applications", Marcel Dekker, New York, 1994.

APPENDIX - A

Table A.1 Line data of the 138 kV 5-bus system, base value = 100 MVA

Line, bus to bus	Length (km)	R (Ω)	X (Ω)	Charging* Mvar
1 to 2	64.4	7.9856	32.0068	4.1
1 to 5	48.3	5.9892	24.0051	3.1
2 to 3	48.3	5.9892	24.0051	3.1
3 to 4	128.7	15.9588	63.9639	8.2
3 to 5	80.5	9.981999	40.0085	5.1
4 to 5	96.5	11.966	47.9605	6.1

$$* \text{ half charging susceptance in } \mu\text{S} = \frac{\text{charging MVAR} \times 10^6}{2\sqrt{3} (V_{LL} \text{ in kV})^2}$$

**Table A.2 P, Q and V at each bus of the 138 kV 5-bus system,
base value = 100 MVA**

Bus No.	Generation		Load		V (p.u.)	ϕ (deg)	Bus type
	P (MW)	Q (Mvar)	P (MW)	Q (Mvar)			
1	65	30	1.04	0	Slack
2	0	0	115	60	1.00	0	PQ
3	180	70	40	1.02	0	PV
4	0	0	70	30	1.00	0	PQ
5	0	0	85	40	1.00	0	PQ

Table A.3 Line data of the 138 kV 14-bus system, base value = 100 MVA

Line, bus to bus	R (p.u.)	X (p.u.)	Half line Charging susceptance (p.u.)
1 to 2	0.01938	0.05917	0.02640
2 to 3	0.04699	0.19797	0.02190
2 to 4	0.05811	0.17632	0.01870
1 to 5	0.05403	0.22304	0.02460
2 to 5	0.05695	0.17388	0.01700
3 to 4	0.06701	0.17103	0.01730
4 to 5	0.01335	0.04211	0.00640
5 to 6	0.0	0.25202	0.0
4 to 7	0.0	0.17615	0.0
7 to 8	0.0	0.17615	0.0
4 to 9	0.0	0.55618	0.0
7 to 9	0.0	0.11001	0.0
9 to 10	0.03181	0.08450	0.0
6 to 11	0.09498	0.19890	0.0
6 to 12	0.12291	0.25581	0.0
6 to 13	0.06615	0.13027	0.0
9 to 14	0.12711	0.27038	0.0
10 to 11	0.08205	0.19207	0.0
12 to 13	0.22092	0.19988	0.0
13 to 14	0.17093	0.34802	0.0

**Table A.4 P, Q and V at each bus of the 138 kV 14-bus system,
base value = 100 MVA**

Bus No.	Generation		Load		V (p.u.)	ϕ (deg)	Bus type
	P (MW)	Q (Mvar)	P (MW)	Q (Mvar)			
1	0	0	1.060	0	Slack
2	240	0	65.10	52.08	1.045	0	PV
3	150	282.60	226.08	1.010	0	PV
4	0	0	143.40	114.72	0	0	PQ
5	0	0	22.80	18.24	0	0	PQ
6	120	33.60	26.88	1.070	0	PV
7	0	0	0	0	0	0	PQ
8	120	0	0	1.090	0	PV
9	0	0	88.50	70.80	0	0	PQ
10	0	0	27.00	21.60	0	0	PQ
11	0	0	10.50	8.40	0	0	PQ
12	0	0	18.30	14.64	0	0	PQ
13	0	0	40.50	32.40	0	0	PQ
14	0	0	44.70	35.76	0	0	PQ

